Title

β-adrenergic-mediated dynamic augmentation of sarcolemmal Ca_V 1.2 clustering and co-operativity in ventricular myocytes.

Journal

The Journal of physiology, 597(8)

ISSN

0022-3751

Authors

Ito, Danica W
Hannigan, Karen I
Ghosh, Debapriya
et al.

Publication Date

2019-04-01

DOI

10.1113/jp277283

Peer reviewed

The Journal of Physiology

β-adrenergic-mediated dynamic augmentation of sarcolemmal $Ca_V1.2$ clustering and co-operativity in ventricular myocytes

Danica W. Ito[1], Karen I. Hannigan[1], Debapriya Ghosh[2], Bing Xu[2], Silvia G. del Villar[1], Yang K. Xiang[2,3], Eamonn J. Dickson[1], Manuel F. Navedo[2] and Rose E. Dixon[1]

[1] *Department of Physiology & Membrane Biology, University of California Davis, Davis, CA, USA*
[2] *Department of Pharmacology, University of California Davis, Davis, CA, USA*
[3] *VA Northern California Health Care System, Mather, CA, USA*

Edited by: Laura Bennet & Bjorn Knollmann

Key points

- Prevailing dogma holds that activation of the β-adrenergic receptor/cAMP/protein kinase A signalling pathway leads to enhanced L-type $Ca_V1.2$ channel activity, resulting in increased Ca^{2+} influx into ventricular myocytes and a positive inotropic response. However, the full mechanistic and molecular details underlying this phenomenon are incompletely understood.
- $Ca_V1.2$ channel clusters decorate T-tubule sarcolemmas of ventricular myocytes. Within clusters, nanometer proximity between channels permits Ca^{2+}-dependent co-operative gating behaviour mediated by physical interactions between adjacent channel C-terminal tails.
- We report that stimulation of cardiomyocytes with isoproterenol, evokes dynamic, protein kinase A-dependent augmentation of $Ca_V1.2$ channel abundance along cardiomyocyte T-tubules, resulting in the appearance of channel 'super-clusters', and enhanced channel co-operativity that amplifies Ca^{2+} influx.
- On the basis of these data, we suggest a new model in which a sub-sarcolemmal pool of pre-synthesized $Ca_V1.2$ channels resides in cardiomyocytes and can be mobilized to the membrane in times of high haemodynamic or metabolic demand, to tune excitation–contraction coupling.

Abstract Voltage-dependent L-type $Ca_V1.2$ channels play an indispensable role in cardiac excitation–contraction coupling. Activation of the β-adrenergic receptor (βAR)/cAMP/protein kinase A (PKA) signalling pathway leads to enhanced $Ca_V1.2$ activity, resulting in increased Ca^{2+} influx into ventricular myocytes and a positive inotropic response. $Ca_V1.2$ channels exhibit a clustered distribution along the T-tubule sarcolemma of ventricular myocytes where nanometer proximity between channels permits Ca^{2+}-dependent co-operative gating behaviour mediated by dynamic, physical, allosteric interactions between adjacent channel C-terminal tails.

Danica Ito is a third year PhD student in the Molecular, Cellular and Integrative Physiology (MCIP) program at the University of California, Davis. She has a BS in Kinesiology and Biology (Westmont College, 2014) and a MS in Exercise Physiology (San Diego State University, 2016). Her ongoing graduate research focuses on the effect of β-adrenergic receptor stimulation on $Ca_V1.2$ channel clustering and co-operativity in ventricular myocytes.

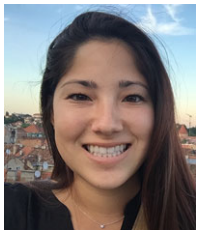

DOI: 10.1113/JP277283

This amplifies Ca^{2+} influx and augments myocyte Ca^{2+} transient and contraction amplitudes. We investigated whether βAR signalling could alter $Ca_V1.2$ channel clustering to facilitate co-operative channel interactions and elevate Ca^{2+} influx in ventricular myocytes. Bimolecular fluorescence complementation experiments reveal that the βAR agonist, isoproterenol (ISO), promotes enhanced $Ca_V1.2$–$Ca_V1.2$ physical interactions. Super-resolution nanoscopy and dynamic channel tracking indicate that these interactions are expedited by enhanced spatial proximity between channels, resulting in the appearance of $Ca_V1.2$ 'super-clusters' along the z-lines of ISO-stimulated cardiomyocytes. The mechanism that leads to super-cluster formation involves rapid, dynamic augmentation of sarcolemmal $Ca_V1.2$ channel abundance after ISO application. Optical and electrophysiological single channel recordings confirm that these newly inserted channels are functional and contribute to overt co-operative gating behaviour of $Ca_V1.2$ channels in ISO stimulated myocytes. The results of the present study reveal a new facet of βAR-mediated regulation of $Ca_V1.2$ channels in the heart and support the novel concept that a pre-synthesized pool of sub-sarcolemmal $Ca_V1.2$ channel-containing vesicles/endosomes resides in cardiomyocytes and can be mobilized to the sarcolemma to tune excitation–contraction coupling to meet metabolic and/or haemodynamic demands.

(Received 8 October 2018; accepted after revision 3 February 2019; first published online 3 February 2019)
Corresponding author Rose E. Dixon: Department of Physiology & Membrane Biology, University of California Davis, One Shields Ave, Tupper Hall Rm 4112, Davis, CA 95616, USA. Email: redickson@ucdavis.edu

Introduction

$Ca_V1.2$ channels are the most abundant L-type calcium channel in the heart, where they represent the primary Ca^{2+} entry pathway across the plasma membrane and are thus indispensable for cardiac excitation–contraction (EC) coupling. Electron microscopy (Franzini-Armstrong *et al.*, 1998), scanning ion-conductance microscopy (Bhargava *et al.*, 2013) and, most recently, super-resolution nanoscopy (Dixon *et al.*, 2015; Dixon *et al.*, 2017) approaches have revealed an inherent tendency of these channels to form discrete clusters on the T-tubule sarcolemma of ventricular myocytes. We have previously reported that groups of channels within these clusters are capable of functionally interacting with their juxtaposed neighbors in a Ca^{2+}-calmodulin (Ca^{2+}/CaM)-dependent manner to open and close together (i.e. co-operative gating) (Dixon *et al.*, 2015). In this scheme, Ca^{2+}/CaM formed when Ca^{2+} flows through the pore of one channel facilitates physical association between adjacent channels by bridging C-terminal pre-IQ motifs. This association allows channels to allosterically communicate with one another, such that the opening of one channel can influence the opening of those physically associated with it. This leads to enhanced open probability (P_o) of the adjoined channels and a resultant amplification of Ca^{2+} influx. An important question that has remained unaddressed is whether co-operative gating behaviour is subject to regulatory control by key signalling pathways.

In the heart, β-adrenergic receptor (βAR) activation initiates a key regulatory pathway, stimulated by the sympathetic nervous system during the fight-or-flight response. This triggers a signalling cascade that results in positive chronotropic, inotropic and lusitropic effects, equipping the heart to deal with the increased haemodynamic and metabolic requirements during physically demanding, stressful or emotional situations. The molecular details of how βAR activation leads to an inotropic response have been the subject of intense investigation for over 50 years after it was first appreciated that catecholamines can vastly enhance Ca^{2+} permeability in cardiomyocytes by increasing the magnitude of the Ca^{2+} current flowing through voltage-dependent L-type Ca^{2+} channels ($Ca_V1.2$) (Tsien *et al.*, 1972; Sperelakis & Schneider, 1976; Reuter & Scholz, 1977). It is now well established that activation of cAMP-dependent protein kinase A (PKA), downstream of βAR stimulation, leads to phosphorylation of $Ca_V1.2$ channels (Osterrieder *et al.*, 1982; Hartzell *et al.*, 1991). This results in increased channel P_o as a result of potentiation of longer-duration 'mode 2' openings (Yue *et al.*, 1990) and an increased number of functional channels (Bean *et al.*, 1984).

Within $Ca_V1.2$ clusters, we have previously reported that channels with a higher P_o dictate the activity of adjoined channels. This was demonstrated in experiments where high P_o Timothy syndrome mutant $Ca_V1.2$ channels ($Ca_V1.2^{G436R}$) were forced to physically interact with lower P_o wild-type (WT) channels using a light activated dimerization system (Dixon *et al.*, 2012). The ensuing amplification of Ca^{2+} influx was attributed to an increase in the P_o of the lower activity WT channels, driven by the adjoined higher activity Timothy syndrome channels. An important implication of this work is that a small number of high P_o channels can have a disproportionately large effect on Ca^{2+} influx

by communicating with other channels in the cluster and exerting a dominant gating influence over them. Applying this same logic to high P_o PKA-phosphorylated channels, a small number of phosphorylated channels could have a big effect on Ca^{2+} influx if they stably interact with lower P_o unphosphorylated channels. However, it is unknown whether βAR signalling can affect $Ca_V1.2$ channel clustering and co-operativity.

Given the reliance of $Ca_V1.2$ co-operativity on Ca^{2+}, we hypothesized that enhanced Ca^{2+} influx through a subset of high P_o PKA-phosphorylated channels, subsequent to βAR stimulation, would promote augmented co-operativity of the channels and produce an amplification of Ca^{2+} influx that could contribute to the inotropic response seen during fight-or-flight. We set out to rigorously test this hypothesis using a unique toolbox including electrophysiology, live-cell imaging, super-resolution nanoscopy, bimolecular fluorescence complementation (BiFC), stepwise photobleaching and Ca^{2+} sparklet recordings. Unexpectedly, our data reveal a mechanistic model that extends beyond the initial assumption that βAR-mediated enhancement of Ca^{2+} influx leads to more $Ca_V1.2$ channel co-operativity. We found that stimulation of cardiomyocytes with the non-selective βAR agonist isoproterenol (ISO), evokes dynamic augmentation of $Ca_V1.2$ channel clustering along the T-tubules of cardiomyocytes, resulting in the appearance of channel 'super-clusters'. Within these super-clusters, enhanced levels of physical proximity promote functional interactions between channels. Dynamic live-cell imaging in freshly isolated adult mouse cardiomyocytes reveals that the ISO-stimulated super-clustering that enhances channel co-operativity occurs at least partly as a result of an increased abundance of the channels at the sarcolemma. On the basis of these data, we suggest a new model in which a readily insertable, sub-sarcolemmal pool of pre-synthesized $Ca_V1.2$ channels resides in cardiomyocytes and can be mobilized to the membrane in times of high haemodynamic or metabolic demand to tune EC-coupling.

Methods

Ethical approval

All procedures involving mice described below, were approved by the University of California Davis Institutional Animal Care and Use Committee (IACUC) and were in accordance with the *Guide for the Care and Use of Laboratory Animals* (National Research Council (US). Committee for the Update of the Guide for the Care and Use of Laboratory Animals. *et al.*, 2011). Animal care and use at UC Davis is accredited and regulated by several independent bodies, including the International Association for Assessment and Accreditation of Laboratory Animal Care, The Office of Laboratory Animal Welfare at the US Department of Health and Human Services Public Health Service, and the United States Department of Agriculture. The authors understand the ethical principles under which the Journal of Physiology operate and confirm that our experiments comply with these principles and with the regulations for reporting animal experiments laid out in (Grundy, 2015).

Isolation of ventricular myocytes

Wild-type C57BL/6J mice were purchased from The Jackson Laboratory (Sacramento, CA, USA) and housed in approved vivarium facilities at UC Davis where they were given *ad libitum* access to food and water. Mice were killed with a single lethal dose of a phenytoin and pentobarbital solution (>100 mg kg^{-1}; Beuthanasia-D Special; Merck Animal Health, Madison, NJ, USA) delivered by I.P. injection. Both male and female young (8–16 weeks old) adult mice were used in the study. Isolations were performed using a Langendorff apparatus as described previously (Dixon *et al.*, 2012; Drum *et al.*, 2013; Dixon *et al.*, 2015). Briefly, hearts were excised and rinsed in a 150 μM EGTA-containing, chilled digestion buffer with the composition: 130 mM NaCl, 5 mM KCl, 3 mM Na-pyruvate, 25 mM Hepes, 0.5 mM $MgCl_2$, 0.33 mM NaH_2PO_4 and 22 mM glucose. The aorta was cannulated and the heart was hung on a Langendorff perfusion apparatus, where it was perfused with warmed (37°C) 150 μM EGTA digestion buffer. When the perfusate was clear of blood, the perfusing solution was changed to a second digestion buffer-based solution (no EGTA) supplemented with 50 μM $CaCl_2$, 0.04 mg mL^{-1} protease (XIV) and 1.4 mg mL^{-1} type 2 collagenase (Worthington Biochemical, Lakewood, NJ, USA) until judged to be adequately digested (appraised by visual inspection of pallor and palpation of the heart to assess loss of rigidity). The atria were then removed via sharp dissection and the remaining ventricles were sliced and placed into 37°C digestion buffer supplemented with 0.96 mg mL^{-1} collagenase, 0.04 mg mL^{-1} protease, 100 μM $CaCl_2$ and 10 mg mL^{-1} BSA. A transfer pipette was used to gently agitate the tissue and release the ventricular myocytes. Cells were left to gravity pellet for 15–20 min. The enzyme-containing supernatant was then removed with a transfer pipette and the pelleted cells were washed in digestion buffer supplemented with 10 mg mL^{-1} BSA and 250 μM $CaCl_2$, and allowed to gravity pellet once more for 15–20 min. The washing supernatant was discarded, and cells were finally suspended in the appropriate solution for the experimental series. For example, for whole cell patch clamp experiments, cells were resuspended at room temperature in Tyrode's solution containing 140 mM NaCl, 5 mM KCl, 10 mM Hepes, 10 mM glucose, 2 mM $CaCl_2$ and 1 mM $MgCl_2$ (pH adjusted to 7.4 with NaOH).

Cell culture and transient transfection

tsA-201 cells originally obtained from Sigma-Aldrich (St Louis, MO, USA) were maintained in a cell culture incubator (37°C, 95:5% O_2:CO_2) in Dulbecco's modified Eagle's medium (DMEM) supplemented with 10% fetal bovine serum and 1% penicillin/streptomycin. Cells were passaged at confluence (every 3–4 days). For heterologous expression of plasmid DNA, cells were grown to 70% confluence and transiently transfected with the cationic transfection reagent, jetPEI (Polyplus Transfection, New York, NY, USA). Cells were incubated in the reagent/DNA mixture for 24 h and re-plated onto the appropriate coverglass the next day, ∼16 h before experiments to allow appropriate recovery and adhesion of the cells.

Plasmid and viral constructs

In the present study, we used pcDNA clones of the pore-forming subunit of the rabbit cardiac isoform of $Ca_V1.2$ α_{1c} (GenBank accession number: NP_001129994.1; provided by William Catterall, University of Washington, Seattle, WA, USA) and rat auxillary subunits $Ca_V\alpha_2\delta$ (AF286488) and $Ca_V\beta_3$ (M88751; provided by Dr Diane Lipscombe; Brown University, Providence, RI, USA). Several $Ca_V1.2$ C-terminal fusion constructs are used in the study including $Ca_V1.2$-EGFP(A206K), $Ca_V1.2$-VC155, $Ca_V1.2$-VN155(I152L) [venus fragments were gifts from Chang-Deng Hu (Kodama & Hu, 2010); Addgene plasmid # 22011 and # 27097; Addgene, Cambridge, MA, USA]. These C-terminal fusion constructs were generated using standard PCR techniques as described previously (Dixon *et al.*, 2015). For expression of $Ca_V1.2$ channels in tsA-201 cells, 800 ng of α_{1c}, 400 ng of $\alpha_2\delta$, 800 ng of β_3 and 200 ng of protein kinase C (PKC)α was added to the jetPEI transfection reagent and the manufacturer's protocol was followed. In BiFC experiments, 400 ng of $Ca_V1.2$-VC155 and of 400 ng $Ca_V1.2$-VN155(I152L) were used to make up the 800 ng of α_{1c}.

In vivo viral transduction of cardiomyocytes

Because cardiomyocytes are impervious to chemical transfection, to visualize $Ca_V1.2$ channels in live cell dynamic imaging and stepwise photobleaching experiments, we used an *in vivo* viral transduction approach. The most cardiotropic adeno-associated virus serotype 9 (AAV9) (Fang *et al.*, 2012) was used to deliver rat $Ca_V\beta_{2a}$ (GenBank accession number: NM_053851.1), with a C-terminal photoactivatable GFP (paGFP) fusion tag via retro-orbital injections. This serotype has been used previously by our group (Dixon *et al.*, 2015) and others (Fang *et al.*, 2012; Drum *et al.*, 2016) to successfully deliver cardiac genes in mice. AAV9-$Ca_V\beta_{2a}$-paGFP was engineered by an in-house core facility (Molecular Construct and Packaging Core) at UC Davis. WT mice were anaesthetized using an isoflurane vaporizer, and a small gauge insulin syringe was used to deliver 4×10^{-12} vg mL^{-1} AAV9-$Ca_V\beta_{2a}$-paGFP into the retro-orbital sinus. Petrolatum ophthalmic ointment was applied to the injected eye and the mice were returned to their cage once they regained consciousness. Injection volumes were restricted to 100–200 μL. Mice were killed 2–5 weeks post-injection and successful transduction was assessed by photo-activating the $Ca_V\beta_{2a}$-paGFP with 405 nm laser light. Prior to photo-activation, no GFP fluorescence emission was detected upon excitation with 488 nm laser light but, after photo-activation, robust GFP fluorescence emission was observed.

BiFC

Physical interactions between $Ca_V1.2$ channels were assayed using BiFC as described previously (Dixon *et al.*, 2015; Moreno *et al.*, 2016). Briefly, this protein–protein interaction assay was performed in tsA-201 cells transfected with 'split venus' tagged channels as described above [$Ca_V1.2$-VC155 and $Ca_V1.2$-VN155(I152L)]. The I152L mutation in the N-terminal portion of the split venus protein has been reported to reduce the level of spontaneous self-assembly between VN and VC, effectively reducing background fluorescence and increasing the signal-to-noise ratio of the assay (Kodama & Hu, 2010). In imaging experiments, tsA-201 cells were transiently transfected with $Ca_V1.2$-VN and $Ca_V1.2$-VC and the relevant auxiliary subunits described above. Total internal reflection fluorescence (TIRF) imaging was then performed on the coverslip plated cells, which were bathed in supplemented DMEM culture medium throughout and maintained at physiological temperature (37°C) for a period of hours. Overnight time series image acquisitions (20 frames min^{-1}) were performed on the cells mounted in a temperature-controlled stage-top CO_2 incubator on a W1-spinning Disk confocal (Andor, Belfast, UK) with a Borealis modification and TIRF module, built around an IX83 inverted microscope (Olympus, Tokyo, Japan) equipped with a 60×/1.49 NA TIRF objective lens. In experiments designed to evaluate the effect of βAR stimulation on physical interactions between $Ca_V1.2$ channels, 100 nM ISO was added at time zero at the onset of imaging. In controls for this experimental series, the overnight imaging proceeded in the absence of ISO. Analysis of the resultant image stacks was performed using ImageJ/Fiji open source image processing software (NIH, Bethesda, MD, USA).

Super-resolution nanoscopy

To remove fluorescent contaminants, #1.5 coverglass (VWR International, Radnor, PA, USA) was sonicated for

20 min in 2 N NaOH, thoroughly rinsed with de-ionized water, and subsequently sterilized and stored in 70% EtOH until use. Isolated myocytes were plated onto laminin (20 μg mL^{-1}; Life Technologies, Carlsbad, CA, USA) and poly-L-lysine (0.01%; Sigma-Aldrich) coated, cleaned coverglass and then placed in a 37° incubator to adhere for 45 min. To stimulate endogenous βARs, adherent myocytes were treated with 100 nM ISO for 8 min, whereas control cells were left untreated for this time period. For labelling experiments on tsA-201 cells, transfected cells expressing $Ca_V1.2$ channels were plated onto cleaned, poly-L-lysine coverslips but otherwise treated in an identical manner to the myocytes.

In experiments designed to test the dependence of $Ca_V1.2$ clustering responses to ISO on PKA activity, from each isolation performed, the groups of coverslip mounted cells that were prepared comprised: (i) control, unstimulated myocytes; (ii) 100 nM ISO-stimulated myocytes (as described above); (iii) myocytes incubated for 10 min with 10 μM H-89 only; (iv) myocytes incubated for 10 min with 10 μM H-89, followed by 8 min with H-89 and 100 nM ISO; (v) myocytes incubated for 1 h with 5 μM protein kinase inhibitor peptide (PKI) only; and (vi) myocytes incubated for 1 h with 5 μM PKI, followed by 8 min with PKI and 100 nM ISO. Groups 1 and 2 served as positive controls to confirm that the super-clustering response was present in cells from each isolation.

For immunostaining, coverglass adherent cells were fixed with ice-cold 100% methanol (Fisher Scientific, Fair Lawn, NJ, USA) for 5 min at –20°C, then thoroughly washed, and blocked for 1 h at room temperature in 50% SEA Block (Thermo Fisher Scientific, Rockford, IL, USA) and 0.5% v/v Triton X-100 (Sigma-Aldrich) in PBS. Primary antibody incubation in rabbit polyclonal anti-$Ca_V1.2$ FP1 antibody (provided by Johannes Hell; Davare *et al.*, 2000; Buonarati *et al.*, 2017) and/or chicken anti-GFP (Life Technologies) was performed overnight at 4°C in antibody solutions diluted to 10 μg mL^{-1} in blocking buffer (20% SEA BLOCK, 0.5% Triton X-100). After thorough washing in PBS, secondary antibody incubation was performed for 1 h at room temperature with Alexa Fluor 647-conjugated donkey anti-rabbit and/or Alexa Fluor 555-conjugated goat anti-chicken (2 μg mL^{-1}; Life Technologies) in PBS. Final thorough washing in PBS was performed to remove excess antibody. Coverglass was then mounted onto glass depression slides (neoLab, Heidelberg, Germany) with a cysteamine (MEA)-catalase/glucose/glucose oxidase (GLOX) imaging buffer containing TN buffer (50 mM Tris pH 8.0, 10 mM NaCl), a GLOX oxygen scavenging system (0.56 mg mL^{-1} glucose oxidase, 34 μg mL^{-1} catalase, 10% w/v glucose) and 100 mM MEA. Twinsil dental glue (Picodent, Wipperfürth, Germany) and aluminum tape (T205-1.0 - AT205; Thorlabs Inc., Newton, NJ, USA) was used to seal the coverglass in place and to exclude oxygen.

Cells were imaged in TIRF mode with 150 nm penetration depth, on a super resolution-ground state depletion (GSD) microscope (Leica Microsystems, Wetzlar, Germany) equipped with an oil-immersion HC PL APO 160 ×/1.43 NA super-resolution objective (Leica), four laser lines (405 nm/30 mW, 488 nm/300 mW, 532 nm/500 mW and 642 nm/500 mW) and an iXon3 electron multiplying charge coupled device (EM-CCD) camera (Andor). Images were collected at a frame rate of 100 Hz for 60,000 frames using Leica Application Suite software. For two-colour images, Alexa-647 was imaged first, followed by Alexa-555. Post-acquisition analysis was performed on images with a 10 nm pixel size and cluster area sizes were determined using binary masks of the images in ImageJ/Fiji.

Dynamic imaging in live cardiomyocytes

Myocytes were isolated from AAV9-$Ca_V\beta_{2a}$-paGFP transduced cardiomyocytes and plated onto poly-L-lysine and laminin-coated glass coverslips. After a 10–15 min settling period to permit cell attachment to the laminin on the coverglass, myocytes were imaged on an IX83 inverted microscope (Olympus) with Cell-TIRF MITICO and an 60×/1.49 NA TIRF objective lens with an additional 1.6× magnification. Light at 405 nm was used to photoactivate the GFP on the $Ca_V\beta_{2a}$ and a 488 nm laser was then used to excite GFP and a 488/561 nm dual band filter cube optimized for TIRF applications (Chroma Technology Corp., Bellows Falls, VT, USA) was used to detect any GFP fluorescence. Cells were perfused with Tyrode's solution (140 mM NaCl, 5 mM KCl, 10 mM Hepes, 10 mM glucose, 2 mM $CaCl_2$ and 1 mM $MgCl_2$; pH adjusted to 7.4 with NaOH) and TIRF time series images were acquired at a rate of 10 frames s^{-1}. The first 300 frames of each experiment were collected under control conditions, then, at frame 301, 100 nM ISO was applied, and the remaining 1200–1600 frames were collected to determine the effect of ISO of channel mobility and expression. ImageJ/Fiji was used for image analysis to quantify the GFP fluorescence in the background subtracted TIRF footprint over the course of the experiments. For display purposes, TIRF images shown in Fig. 3*A* (see also the Supporting information, Movie S1) were stabilized to compensate for cell movement using the 'Image Stabilizer' plugin for ImageJ. A 10-pixel rolling ball background subtraction was applied, followed by 10 frame moving average and, finally, a minimum intensity projection was subtracted from all frames in the stack. In addition, super-resolution reconstructions were generated from the raw, unprocessed TIRF time series images using the NanoJ-SRRF plugin freely available in ImageJ/Fiji (Gustafsson *et al.*, 2016). The super-resolution radial fluctuations (SRRF) algorithm can be used to analyse conventional diffraction-limited images (such as our TIRF images) to generate super-resolution

reconstructions by splitting the individual pixels of the image into smaller units and then examining each pixel for radiality. The idea is that fluorophores emit from a point source, convolved with a point spread function that has an intrinsic radiality. This distinguishes them from the background, which should not have radiality. The algorithm then highlights the pixels with high radiality to achieve a super-resolution reconstruction. Resolutions in the range of ∼64 nm have been reported using this algorithm on conventional TIRF images (Gustafsson *et al.*, 2016).

Stepwise photobleaching

Isolated, coverglass-plated AAV9-$Ca_V\beta_{2a}$-paGFP transduced myocytes were fixed for 10 min in 4% paraformaldehyde, washed and subsequently imaged on a DMI6000 B TIRF microscope (Leica) using a 160×/1.43 NA objective. The paGFP was photoactivated with a 405 nm laser and then excited with 488 nm laser light illumination during the collection of 2000 frame image stacks acquired at a rate of 30 Hz. Data were analysed and bleaching steps were manually counted as described previously (Dixon *et al.*, 2015).

Electrophysiology

Single $Ca_V1.2$ channel currents (i_{Ca}) were recorded from transiently transfected tsA-201 cells using the cell-attached configuration of the patch clamp technique. Borosilicate glass pipettes with 5–10 MΩ resistance were filled with a solution containing 20 mM $CaCl_2$, 10 mM Hepes and 500 nM BayK-8644 (pH adjusted to 7.2 using TEA-Cl) and used to obtain a gigaseal. Cells were bathed in a high K^+ solution (145 mM KCl, 2 mM $MgCl_2$, 0.1 mM $CaCl_2$, 10 mM Hepes and 10 mM glucose; pH adjusted to 7.3 with KOH) to set the membrane potential to ∼0 mV. Currents were elicited using a step depolarization protocol from a holding potential of –80 mV to a test potential of –30 mV, and were sampled at a frequency of 10–20 kHz, low-pass–filtered at 2 kHz using an Axopatch 200B amplifier (Molecular Devices, Sunnyvale, CA, USA), digitized using a Digidata 1550B plus Humsilencer (Molecular Devices) and acquired using pClamp, version 10.7 (Molecular Devices). Clampfit software (Molecular Devices) was used to detect single channel openings, measure i_{Ca} amplitudes, construct all-points histograms and determine channel P_o. The average single channel current was calculated by taking the mean of the difference between each of the multicomponent Gaussian-fitted peaks in the all-points histograms for each data set. In this calculation, we ignore the prominent subconductance state (∼0.25 pA), which has been documented previously (Chen-Izu, 2010). Our assumption that the ∼0.5 pA state is the maximum conductance for a single channel opening at –30 mV using 20 mM Ca^{2+} in the patch pipette is in agreement with previously published studies (Rubart *et al.*, 1996; Josephson *et al.*, 2002). Ensemble current averages were generated from the detected events. The membrane potentials referred to in the Results have been corrected for liquid junction potential. All experiments were performed at room temperature (22–25°C) unless otherwise stated. The same approach was used to record i_{Ca} from isolated ventricular myocytes, except that the external solution was 0 mM Ca^{2+} Tyrode's solution until a gigaseal was obtained, at which point the perfusate was switched to the high K^+ solution described above.

Whole cell currents (I_{Ca}) were also recorded from tsA-201 cells before and after application of 100 nM ISO to attempt to visualize a recapitulation of the βAR-mediated regulation of the channels seen robustly in ventricular myocytes. In these experiments, pipettes were filled with a Cs-based internal solution (7 mM Cs-aspartate, 20 mM CsCl, 1 mM $MgCl_2$, 10 mM Hepes, 10 mM EGTA and 5 mM MgATP; pH adjusted to 7.2 with CsOH) and bathed in an external solution with the composition: 5 mM CsCl, 10 mM Hepes, 10 mM glucose, 113 mM NMDG, 1 mM $MgCl_2$ and 20 mM $CaCl_2$ (pH adjusted to 7.4 with HCl). Currents were elicited with a series of 300 ms depolarizing pulses from a holding potential of −80 mV to test potentials ranging from −60 to +80 mV. The resultant current–voltage relationships were plotted using Prism (GraphPad Software Inc., La Jolla, CA, USA). The voltage-dependence of conductance was obtained by converting currents to conductances using the equation, $G = I_{Ca}/[\text{test pulse potential} - \text{reversal potential of } I_{Ca}]$, normalizing ($G/G_{max}$) and plotting conductance *vs.* the test potential. Gating currents were also measured in tsA-201 cells before and after 100 nM ISO, by first running an *I–V* protocol, and calculating the reversal potential for Ca^{2+} from the *I–V* plot. Leak and capacitive currents were compensated for. The voltage protocol was then modified to step to E_{Ca} and record currents in the absence of ion flux, leaving only the gating current. We integrated the gating current to obtain the ON gating charge (Q_{ON}).

I_{Ca} recording in ventricular myocytes was performed as described previously (Cheng *et al.*, 2011; Dixon *et al.*, 2015). Briefly, the cells were perfused with Tyrode's solution prior to successful conversion to the whole-cell configuration, when the external solution was replaced with 5 mM CsCl, 10 mM Hepes, 10 mM glucose, 140 mM NMDG, 1 mM $MgCl_2$ and 2 mM $CaCl_2$ (pH adjusted to 7.4 with HCl). The internal pipette solution was the same Cs-based solution described above for tsA-201 I_{Ca} recordings. Currents were elicited with 300 ms long depolarizations from –80 mV to test potentials ranging from –40 mV to +50 mV. An additional 100 ms

long voltage step to –40 mV immediately preceded the depolarization pulses to inactivate voltage-gated Na^+ channels.

Ca^{2+} sparklet recording and analysis

Optical recordings of $Ca_V1.2$ channel openings in transiently transfected tsA-201 cells or ventricular myocytes were performed by voltage clamping the cells at –80 mV using the whole cell configuration of the patch clamp technique, and dialysing in the tripotassium salt of the Ca^{2+} indicator Rhod-2 (200 μM) via the patch pipette. The membrane and near membrane area of these cells were imaged using an IX83 inverted microscope (Olympus) with Cell-TIRF MITICO and an 60×/1.49 NA TIRF objective lens. This enabled capture of sub-sarcolemmal Ca^{2+} signals (Ca^{2+} sparklets). Stacks of images were acquired at a rate of ∼100 Hz using an iXon Ultra 888 back thinned EM-CCD camera (Andor). Cells were continuously perfused with the 20 mM Ca^{2+}, 10 mM EGTA external solution described above. For experiments performed in ventricular myocytes, the sarco/endoplasmic reticulum Ca^{2+}-ATPase pump inhibitor thapsigargin (10 μM) was used to reduce SR Ca^{2+} load and prevent Ca^{2+} sparks to ensure specific recording of Ca^{2+} sparklets (Zima *et al.*, 2008). TIRF imaging to create a shallow evanescent field, along with the Ca^{2+} indicator and EGTA buffer combination, permits the fluorescence labelling of Ca^{2+} as it enters the cell and binds to the fast Ca^{2+} indicator Rhod-2, before EGTA buffers Ca^{2+} to restrict the signal to the point of entry. Fluorescence signals were converted to intracellular Ca^{2+} concentrations using the F_{max} equation (Maravall *et al.*, 2000). Sparklets were identified and their time courses analysed using a custom-written MATLAB script (MathWorks Inc., Natick, MA, USA). Sparklet activity was quantified as nP_s, where n is the number of quantal levels and P_s is the probability that a sparklet occurs. Another parameter, sparklet site density, is defined as the number of observable sparklet sites per unit of cell footprint area.

Western blots

Wild-type C57BL/6J mice were administered either an I.P. injection of saline (control) or 10 mg kg^{-1} ISO. After 20 min, mice were killed with an anaesthetic overdose of isoflurane (5%) and hearts were collected via sharp dissection. The hearts were subsequently homogenized in osmotic lysis buffer (25 mmol L^{-1} Tris-HCl, pH 7.4, 5 mmol L^{-1} EDTA, pH 8.0, 1 mmol L^{-1} phenylmethane sulphonyl fluoride (PMSF), 2 μg mL^{-1} aprotinin and 2 μg mL^{-1} leupeptin). Cell debris and nuclei were removed by centrifugation at 950 *g* for 5 min at 4°C. The supernatant was then centrifuged at 37,500 *g* for 30 min at 4°C using a Type 70.1 Ti Fixed-Angle Titanium Rotor (Beckman Coulter, Indianapolis, IN, USA). Pellets representing the sarcolemma/plasma membrane (PM) fraction were resuspended in Triton lysis buffer (25 mmol L^{-1} Hepes, pH 7.4, 5 mmol L^{-1} EDTA, 150 mmol L^{-1} NaCl, 1% Triton X-100, and protease inhibitors containing 2 mmol L^{-1} Na_3VO_4, 1 mmol L^{-1} PMSF, 10 mmol L^{-1} NaF, 10 μg mL^{-1} aprotinin, 5 mmol L^{-1} bestatin, 10 μg mL^{-1} leupeptin and 2 μg mL^{-1} pepstain A) for western blotting. The supernatant was further centrifuged at 200,000 *g* for 1 h at 4°C; the pellets obtained in this step contained internal membrane compartment fractions and were resuspended in Triton lysis buffer, as described above, for western blotting. Equal amounts of protein were resolved by SDS-PAGE and detected with anti-$Ca_V1.2$ FP1 antibody, anti-Rab4A antibody (D-20; rabbit polyclonal IgG; SC-312; Santa Cruz Biotechnology, Dallas, TX, USA) and anti-insulin receptor β antibody (L55B10; mouse monoclonal IgG1; 3020; Cell Signaling Technology, Danvers, MA, USA). All primary antibodies were revealed with IRDye 800 CW secondary antibodies using Odyssey detection system (Li-Cor Biosciences, Lincoln, NE, USA). The optical density of the bands was analysed with ImageJ (https://imagej.nih.gov/ij).

Chemicals and statistical analysis

Chemical reagents were obtained from Sigma-Aldrich unless otherwise stated. Data are reported as the mean ± SEM. *N* reflects the number of animals used in a dataset, whereas *n* reflects the number of cells. Actual *P* values are provided unless the *P* value is extremely low, when it is simply stated as $P < 0.001$. Comparison of paired datasets was performed using Student's *t* tests if the data passed a normality test. Otherwise, a non-parametric test was performed. $P < 0.05$ was considered statistically significant ($^*P < 0.05$; $^{**}P < 0.01$; $^{***}P < 0.001$).

Results

βAR stimulation promotes enhanced $Ca_V1.2$–$Ca_V1.2$ channel interactions

$Ca_V1.2$ channel co-operativity requires physical interactions between adjacent channels (Dixon *et al.*, 2012; Dixon *et al.*, 2015). Thus, our first experimental series investigated the effect of βAR stimulation on $Ca_V1.2$–$Ca_V1.2$ channel interactions using an optical assay of protein–protein interactions, namely BiFC (Fig. 1). We have previously used this approach to assay the Ca^{2+} and CaM-dependence of $Ca_V1.2$–$Ca_V1.2$ interactions in tsA201 cells (Dixon *et al.*, 2015; Moreno *et al.*, 2016). For this, we generated two fusion proteins, $Ca_V1.2$-VC155 and $Ca_V1.2$-VN155(I152L), by fusing the N- or C- terminal fragment of the venus fluorescent protein (FP) onto the

C-terminal of the $Ca_V1.2$ α_{1c} subunit. In the present study, the channels were transiently transfected into tsA201 cells and the degree of venus reconstitution was assayed under control and ISO stimulated conditions. BiFC complex formation occurs when the two fragments of the FP interact and fold upon association. This leads to the irreversible reconstitution of the mature venus FP and a visible fluorescence read-out of the protein–protein interaction in the form of venus fluorescence as summarized by the cartoon in Fig. 1*A*. The time taken for protein folding varies but can be quite a protracted affair as demonstrated previously in a study examining the kinetics of the YFP BiFC complex formation, which reported that, although complexes could be appreciated in as little as 10 min, they continued to form over a period of at least 8 h (Robida & Kerppola, 2009). Because folding of venus fragments occurs at an accelerated rate compared to YFP (Nagai *et al.*, 2002), we therefore monitored venus fluorescence from the TIRF footprint of tsA201 cells expressing $Ca_V1.2$-VN155(I152L) and $Ca_V1.2$-VC155 over a period of 2 h in cells maintained at 37°C with 95:5 O_2:CO_2 in a stage top incubator. Under control conditions, venus F/F_0 increased with a τ of 18.57 min (n = 18) (Fig. 1*B* and *D*). Spontaneous interactions such as these in unstimulated cells are not unexpected, given that tsA-201 cells have quite a depolarized resting

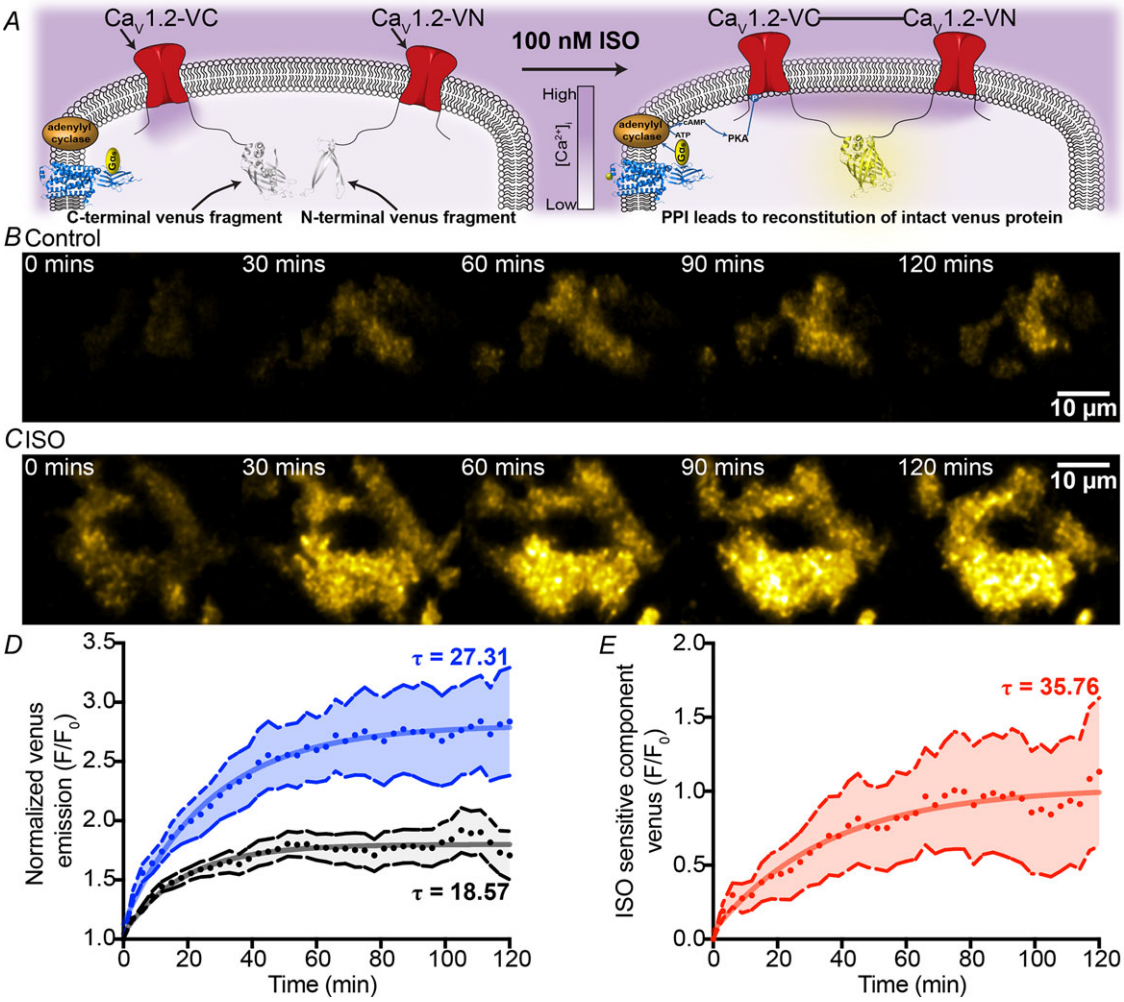

Figure 1. β-AR stimulation promotes enhanced $Ca_V1.2$–$Ca_V1.2$ channel interactions
A, BiFC experimental strategy. Left: non-interacting channels with a C-terminal fusion of N- or C-terminal venus FP fragments. Right: application of 100 nM ISO stimulates endogenous β_2-ARs, increasing cAMP and activating PKA that acts on the channels to promote physical interactions, resulting in reconstitution of the intact venus protein and fluorescence emission. *B*–*C*, TIRF image time series obtained from tsA-201 cells expressing $Ca_V1.2$-VN and $Ca_V1.2$-VC, incubated at 37°C without (control) (*B*) or with 100 nM ISO (*C*). Images received a one pixel median filter for display purposes. *D*, time course of the changes in normalized venus fluorescence emission (F/F_0) over 2 h for control (black/grey) and ISO stimulated (blue) conditions. Circles indicate mean venus intensity at each time point, dashed lines and area fills indicate the SEM. Data were fit with mono-exponential functions to calculate the time constant (τ) of the interactions. *E*, time course of the ISO sensitive component of the interactions.

membrane potential of ~–25 mV (Kirkton & Bursac, 2011), which would permit a small amount of Ca^{2+} influx through these voltage-gated channels and could facilitate Ca^{2+}-dependent physical interactions. Application of 100 nM ISO (n = 10) at the onset of the experiment stimulated endogenous β_2ARs (Atwood *et al.*, 2011) and resulted in a significantly larger increase in venus F/F_0 compared to the control (ISO = 2.84 ± 0.46 F/F_0 *vs.* control = 1.71 ± 0.21 F/F_0; P = 0.015) (Fig. 1*C* and *D*). $Ca_V1.2$–$Ca_V1.2$ interactions increased steadily over the time-course of the experiment with a τ of 27.31 min, notably slower than that of the unstimulated control. To calculate the ISO-sensitive component of the interactions, we subtracted the control data from the ISO data to generate the data in Fig. 1*E*. The time constant of the ISO-sensitive interactions was 35.76 min. Collectively, these BiFC data suggest that β_2AR stimulation triggers enhanced levels of physical C-tail to C-tail association between $Ca_V1.2$ channels.

ISO promotes super-clustering of $Ca_V1.2$ channels

Enhanced spatial proximity between channels would be predicted to increase $Ca_V1.2$–$Ca_V1.2$ interaction probability. Thus, to investigate the spatial distribution of $Ca_V1.2$ channels under control and ISO stimulated conditions, we examined fixed, anti-$Ca_V1.2$ immunostained cardiomyocytes and transfected tsA-201 cells using super-resolution nanoscopy. Under control conditions, the average $Ca_V1.2$ cluster area in ventricular myocytes was 3698 ± 59 nm^2 (N = 11, n = 54 cells) (Fig. 2*A* and *D*). In myocytes stimulated with 100 nM ISO for 8 min prior

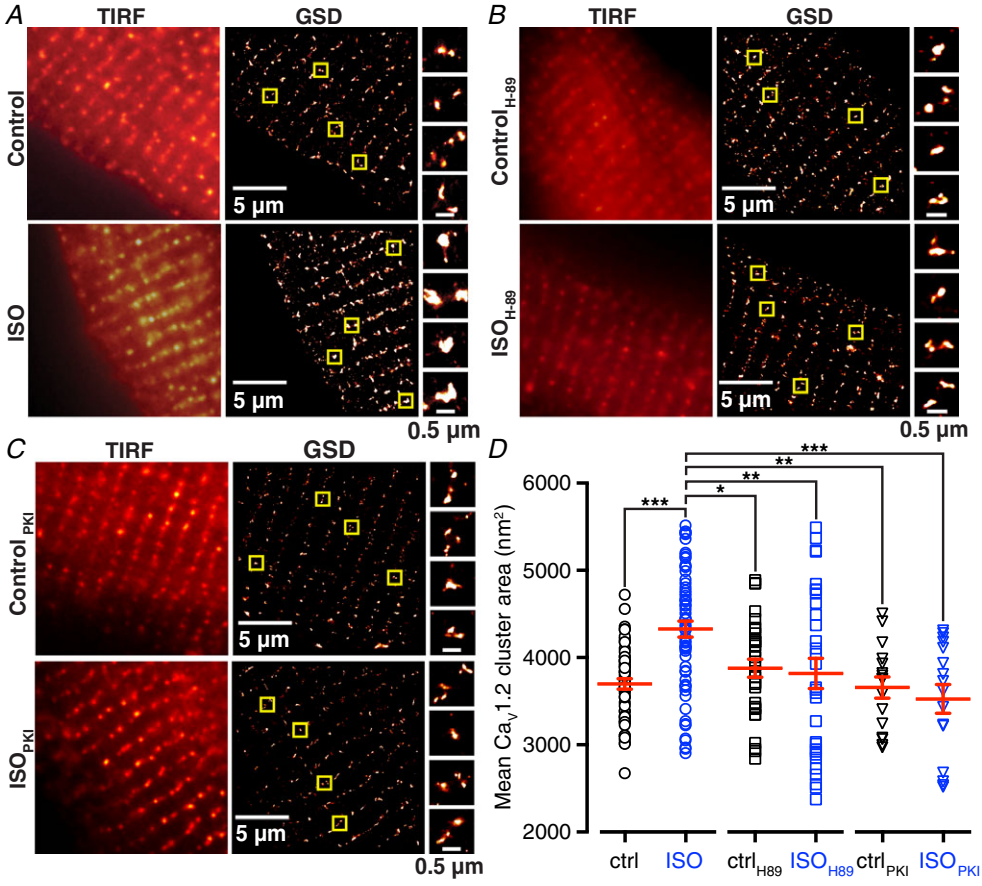

Figure 2. ISO-induced 'super-clustering' of $Ca_V1.2$ is mediated by PKA
A, diffraction-limited TIRF (left column) and GSD (right column) images of a control (top row) or 100 nM ISO-stimulated (bottom row), fixed, adult mouse ventricular cardiomyocyte immunostained to examine $Ca_V1.2$ channel distribution. Images were pseudocoloured 'red hot' and received a one pixel median filter for display purposes. Yellow boxes indicate the location of the zoomed-in regions displayed on far right. *B* and *C*, same layout format in myocytes pretreated with 10 µM H-89 (*B*) or 5 µM PKI (*C*). *D*, aligned dot plot showing mean $Ca_V1.2$ channel cluster areas in control (black circles) and ISO-stimulated (blue circles) myocytes in H-89 pre-treated myocytes under control (black squares) or ISO-stimulated (blue squares) conditions and in PKI pre-treated myocytes control (black triangles) or ISO-stimulated (blue triangles) conditions. Red lines indicate the mean for each dataset and error bars indicate the SEM.

to fixation, the average $Ca_V1.2$ cluster area was ∼17% larger than controls (4327 ± 92 nm^2, $N = 11$, $n = 61$) (Fig. 2*A* and *D*), with large 'super-clusters' evident in the GSD images. A significant, ISO-induced augmentation in $Ca_V1.2$ channel cluster area was also evident in $Ca_V1.2$ expressing tsA-201 cells (Fig. 3). These results suggest that βAR stimulation initiates a nanoscale redistribution of $Ca_V1.2$ channels within cardiomyocytes and tsA-201 cells that favours enhanced levels of physical interactions between the channels.

Super-clustering in ventricular myocytes is PKA-dependent

To determine whether the observed ISO-induced super-clustering of $Ca_V1.2$ channels depended on PKA activity, further super-resolution nanoscopy experiments were performed on isolated ventricular myocytes in the absence and presence of the PKA inhibitors H-89 (Hidaka & Kobayashi, 1992) or the more specific, membrane-permeable, myristoylated 14–22 amide (referred to in the present study as PKI) (Murray, 2008). Positive controls were performed on each batch of isolated cells to confirm that the super-clustering response to ISO was present in the absence of PKA inhibition and to give added strength to any observed effects. Average $Ca_V1.2$ channel cluster area was not significantly altered by ISO treatment when PKA was inhibited with either 10 μM H-89 ($control_{H\text{-}89}$ 3879 ± 103 nm^2, $n = 31$; $ISO_{H\text{-}89}$ 3818 ± 172 nm^2, $n = 31$; $P = 0.99$, $N = 4$) (Fig. 2*B* and *D*) or 5 μM PKI ($control_{PKI}$ 3657 ± 123 nm^2, $n = 16$; ISO_{PKI} 3526 ± 165 nm^2, $n = 16$; $P = 0.99$, $N = 3$) (Fig. 2*C* and *D*). A one-way ANOVA with Tukey's multiple comparison test indicated that all of the PKA-inhibited groups were not significantly different from the control (no inhibitor) group, although they were significantly different from the ISO-stimulated (no inhibitor) group (Fig. 2*D*). These results suggest that the super-clustering response to ISO is a PKA-dependent phenomenon.

ISO-stimulated dynamic augmentation of sarcolemmal channel abundance

There are at least two possible, not necessarily mutually exclusive mechanisms that could explain the enhanced $Ca_V1.2$ clustering response to ISO. First, smaller $Ca_V1.2$ channel clusters could fuse together to form super-clusters. Alternatively, enhanced trafficking and insertion of $Ca_V1.2$ channels into the sarcolemma could explain these results. To distinguish between these two scenarios, we aimed to examine the dynamics of $Ca_V1.2$ channels in freshly dissociated cardiomyocytes. These cells are impervious to chemical transfection techniques and rapidly lose their unique ion channel complement and specialized architecture as they dedifferentiate in culture (Louch *et al.*, 2011). Thus, expression of FP-tagged channels in cardiomyocytes to monitor their trafficking and dynamics presents a technical challenge. We have previously demonstrated successful transduction of mouse cardiomyocytes *in vivo* with various FP-tagged constructs using retro-orbital injections of AAV9 (Dixon *et al.*, 2015; Drum *et al.*, 2016; Moreno *et al.*, 2016). This approach allows us to circumvent the need to culture the cells and lets the transduction proceed *in vivo*. A limitation of AAV9s is their restrictive packaging capacity of ∼5 kb (Vinge *et al.*, 2008; Louch *et al.*, 2011). This precludes expression of the ∼6.6 kb α_{1c} pore-forming subunit of the channel. We therefore chose to package one of the smaller (1.8 kb) auxiliary subunits of the $Ca_V1.2$ channel, $Ca_V\beta_{2a}$, which binds to the α_{1c} with a 1:1 stoichiometry (Dalton *et al.*, 2005). We fused $Ca_V\beta_{2a}$ to a paGFP to permit live-cell tracking of the subunit when expressed in cardiomyocytes. Note that the recent use of this approach by our group revealed $Ca_V\beta_{2a}$-associated fluorescence with similar cluster size and distributions to those observed in the present study (Dixon *et al.*, 2015).

Transduced cardiomyocytes were imaged using TIRF microscopy to narrow the evanescent field and focus on channels at the plasma membrane. After photoactivation, a time series of TIRF images was collected at a rate of 10 frames s^{-1} to monitor $Ca_V\beta_{2a}$-paGFP movements during an initial 300 frame control period before wash-in of 100 nM ISO and a subsequent 1200–1600 frames to

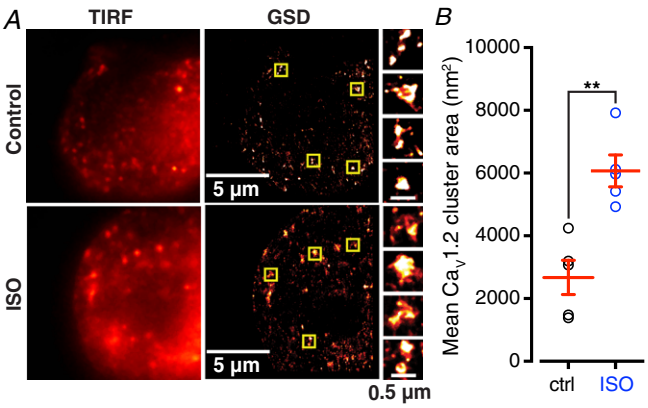

Figure 3. ISO augments $Ca_V1.2$ channel cluster areas in tsA-201 cell plasma membranes
A, diffraction-limited TIRF (left column) and GSD (right column) images of control (top row) and 100 nM ISO-stimulated (bottom row), fixed, tsA-201 cells expressing $Ca_V1.2$ channels, immunostained to examine the channel distribution. Images were pseudocoloured 'red hot' and received a one pixel median filter for display purposes. Yellow boxes indicate the location of the zoomed-in regions displayed on far right. *B*, aligned dot plot showing mean $Ca_V1.2$ channel cluster areas in control (black circles) and ISO-stimulated (blue circles) tsA-201 cells. Red lines indicate the mean for each dataset and error bars indicate the SEM.

capture the movements in the presence of this agonist. In the mean intensity analysis, presented in Fig. 4*C*, the sum of the intensity values of all the pixels in the TIRF footprint of the cell is divided by the number of pixels in the footprint. To obtain the F/F_0, the values are further normalized to the mean intensity measured in the first frame of the time series. If the super-clustering response was generated solely by individual or small aggregates of $Ca_V\beta_{2a}$-paGFP fusing with one another to form larger, more readily detectable clusters then one would predict that the mean intensity would not change over the course of the experiment, rather the distribution of the existing FPs would be altered. We find instead that ISO stimulated a dynamic increase in $Ca_V\beta_{2a}$-paGFP abundance in the TIRF footprint of cardiomyocytes ($N = 2$, $n = 6$) (Fig. 4*A–C*; see also the Supporting information, Movie S1). Indeed, the average maximal response to ISO amounted to a 44.9 ± 6.2% increase (F/F_0) within the time-course of the experiment (Fig. 4*C*). This dynamic elevation in GFP intensity in the TIRF footprint can be visualized (see the Supporting information, Movie S1) as the appearance of discrete clusters of fluorescence presumably originating from a site deeper within the cell, outside the TIRF illumination field. This finding does not preclude the possibility that there is some aggregation of already present $Ca_V\beta_{2a}$-paGFP, although our data suggest that this does not form the major basis of the super-clustering response.

To further investigate whether this dynamic channel insertion results in super-clustering, we generated super-resolution reconstructions from our TIRF image stacks using the NanoJ-SRRF plugin for ImageJ, allowing us to resolve discrete clusters of $Ca_V\beta_{2a}$-paGFP (Fig. 4*A–C*) (Gustafsson *et al.*, 2016). This open source plugin permits the post-acquisition extraction of live-cell super-resolution information from stacks of images acquired using diffraction-limited microscopy techniques such as TIRF or confocal microscopy. It is clear from these images that myocyte stimulation with ISO triggers dynamic augmentation of sarcolemmal $Ca_V\beta_{2a}$-paGFP expression and super-clustering.

Overexpression of $Ca_V\beta_{2a}$ in cardiomyocytes does not affect basal $Ca_V1.2$ clustering

Because we are using an overexpression paradigm to visualize $Ca_V\beta_{2a}$-paGFP in these cells, on a background with native, non-fluorescent $Ca_V\beta_{2a}$, we are at best, observing only a small subset of the $Ca_V\beta_{2a}$ expression on the sarcolemma. Endogenously expressed $Ca_V\beta_{2a}$ probably constitutes the vast majority of the population of this subunit interacting with the α_{1c}. This probably explains why complete T-tubule localization pattern is not not seen for $Ca_V\beta_{2a}$-paGFP. However, upon stimulation with ISO, examination of the super-resolution reconstructions revealed discrete regions of the cells in which the pattern of $Ca_V\beta_{2a}$-paGFP expression is consistent with the expected physiological range of sarcomere lengths and a separation of 1.6–2.3 μm between T-tubules (Fig. 4*B*).

To further examine the distribution of transduced $Ca_V\beta_{2a}$-paGFP and its relative colocalization with endogenous $Ca_V1.2$ channels, super-resolution GSD experiments were performed before and after ISO using an anti-$Ca_V1.2$ and anti-GFP double labelling approach. In this dataset, the mean $Ca_V1.2$ channel cluster area was 3253 ± 157 nm^2 under control conditions ($n = 5$), swelling to 4086 ± 151 nm^2 in ISO treated myocytes ($n = 6$, $P = 0.004$) (Fig. 4*D–F*). The magnitude of the response to ISO (~26%), and the basal and ISO stimulated cluster areas were not significantly different from those observed in control untransduced cells ($P = 0.058$), indicating that overexpression of the $Ca_V\beta_{2a}$ subunit did not itself artificially increase basal channel cluster sizes or the dynamic augmentation response to ISO. As in the dynamic imaging experiments, the distribution of $Ca_V\beta_{2a}$-paGFP did not display a complete T-tubule localization pattern, although the added perspective given by the $Ca_V1.2$ channel co-label confirms that the transduced subunits are indeed occupying positions along the T-tubules where they colocalize with $Ca_V1.2$ clusters (Fig. 4*D–F*). Stimulation with 100 nM ISO prior to fixation also increased the mean $Ca_V\beta_{2a}$-paGFP cluster area from 4141 ± 535 nm^2 in control ($n = 5$) to 5675 ± 453 nm^2 ($n = 6$; $P = 0.026$), reflecting the increased expression and larger post-ISO $Ca_V\beta_{2a}$-paGFP cluster sizes observed in the dynamic experiments.

Further quantification of the $Ca_V\beta_{2a}$-paGFP response to ISO was performed by examining single-particle photobleaching in transduced cardiomyocytes (Ulbrich & Isacoff, 2007). The number of $Ca_V\beta_{2a}$-paGFP molecules within individual clusters was determined by counting the number of steps in the fluorescence as the fused paGFP tag bleached. Discrete bleaching steps become difficult to resolve in clusters containing more than five channels (Ulbrich & Isacoff, 2007). Therefore, instead, we measured the amplitude of a single paGFP bleaching-step by constructing an all-points histogram of all resolvable bleaching-steps (104 clusters, $n = 11$ cells). The cluster distribution was then fit with a two-component Gaussian function, and the centre of the peak corresponding to the smaller step size (23.61 ± 0.32 AIU) was assumed to represent the quantal amplitude of a single paGFP photobleaching-step (Fig 5*A*). The number of $Ca_V\beta_{2a}$-paGFP molecules per cluster was then calculated by subtracting the initial from the final fluorescence intensity of each cluster and dividing the result by the quantal value. An important caveat of this experiment is that we may be underestimating the number of channels per cluster. The first underestimation factor is a result

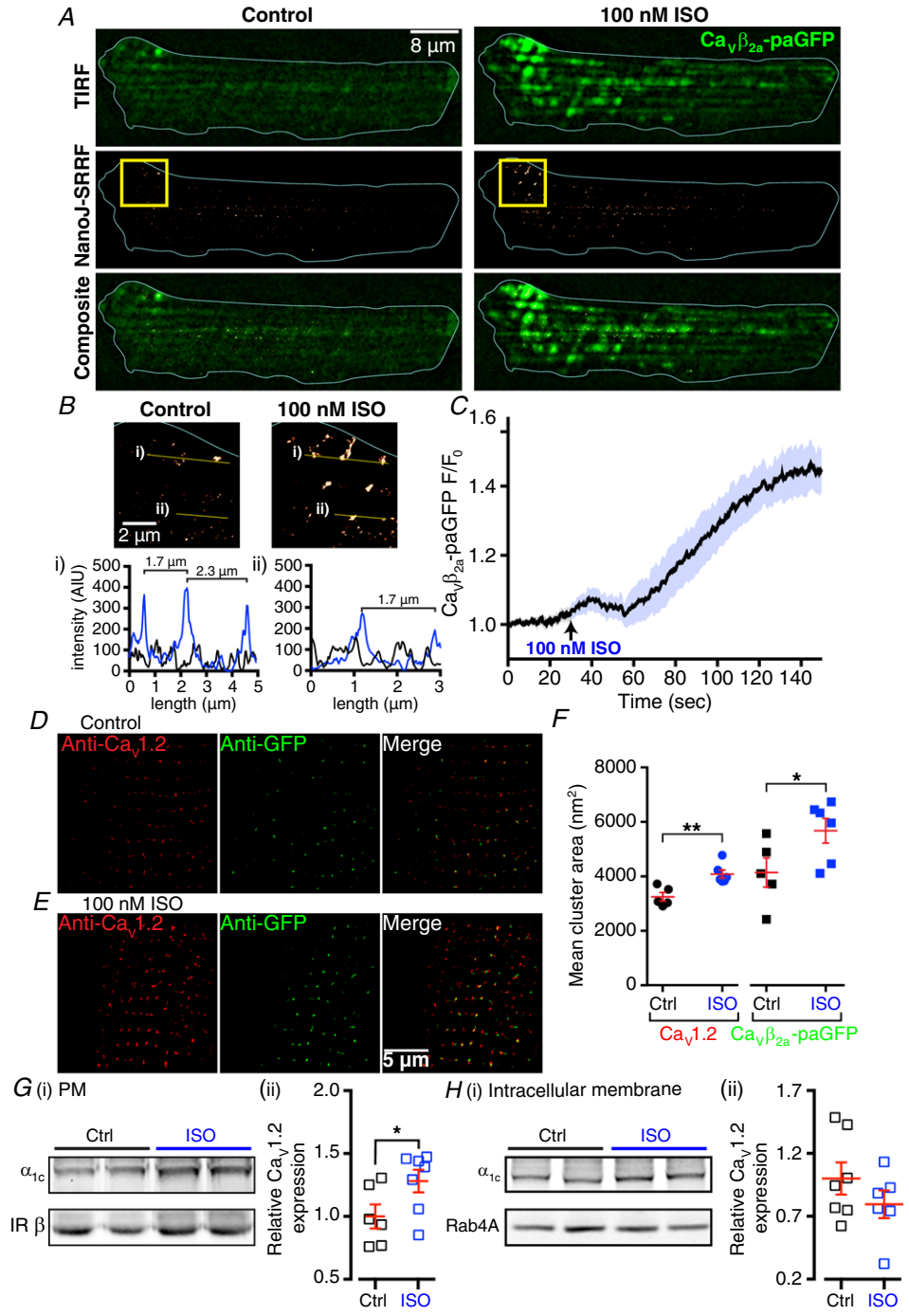

Figure 4. ISO stimulates dynamic augmentation of $Ca_V1.2$ channel sarcolemmal abundance
A, top: diffraction-limited TIRF images of photoactivated GFP fluorescence emission from $Ca_V\beta_{2a}$-paGFP transduced cardiomyocytes before (left) and after application of 100 nM ISO (right). Middle row: NanoJ-SRRF generated super-resolution images of the same cell. Bottom row: composites of the TIRF and NanoJ-SRRF images. *B*, magnified NanoJ-SRRF images before and after ISO. Locations on the larger images are indicated by yellow boxes in (*A*). Intensity plot profiles across the dotted yellow lines labelled (i) and (ii) are displayed below where the black trace represents the control plot and the blue represents a plot from the same region after ISO. *C*, time course of the changes in normalized photoactivated $Ca_V\beta_{2a}$-paGFP emission (F/F_0) during a 30 s control period and a subsequent 120 s exposure to ISO. *D–E*, super-resolution images of fixed control (*D*) or ISO-stimulated (*E*) ventricular myocytes double labelled to show $Ca_V1.2$ (left) and GFP (middle) distribution. Colocalized pixels appear yellow in the merged image (right) and confirm t-tubule localization of $Ca_V\beta_{2a}$-paGFP. *F*, scatter plot showing the mean $Ca_V1.2$ and $Ca_V\beta_{2a}$-paGFP cluster sizes, in control (black) and ISO-stimulated (blue) ventricular myocytes. *G* and *H*, (i) representative western blots illustrating the detection of $Ca_V1.2$ α_{1c} and insulin receptor β in plasma membrane

fractions (*G*) or $Ca_V1.2$ α_{1c} and Rab4A in intracellular membrane fractions (*H*) isolated from whole heart lysates obtained from mice 20 min post I.P. injection with either saline (control) or 10 mg kg^{-1} ISO. *G* and *H*, (ii) scatter plots showing the relative $Ca_V1.2$ channel expression in each fraction.

of the non-unity (~0.8 based on previous studies) probability that any single GFP molecule is fluorescent (Ulbrich & Isacoff, 2007). The second factor is the presence of endogenous $Ca_V\beta$ subunits that, as discussed above, are probably associated with the majority of channels and thus with this approach, we can only make a reasonable estimation of the minimum number of channels per cluster. With that said, we did find a significantly altered distribution of the channel occupancy in sarcolemmal clusters after application of 100 nM ISO (Fig. 5*B*). The mean number of $Ca_V\beta_{2a}$-paGFP molecules per cluster was 6.62 ± 0.16 in unstimulated control myocytes (calculated from 983 spots; $n = 14$, $N = 3$). The frequency distribution of all clusters examined revealed a dominant population at 5.17 ± 0.07 $Ca_V\beta_{2a}$-paGFP per cluster (Fig. 5*B* and *C*). With ISO stimulation, the mean number of $Ca_V\beta_{2a}$-paGFP per cluster was 8.75 ± 0.22 (calculated from 1,162 spots, $n = 15$, $N = 3$), representing a 32% increase compared to controls. Frequency distribution analysis revealed two dominant populations of clusters. The first was a similar size to control with 4.02 ± 0.05 $Ca_V\beta_{2a}$-paGFP molecules per cluster, whereas the second had 8.33 ± 0.23 (Fig. 5*B* and *C*). These results provide further validation of our dynamic imaging data and suggest that βAR stimulation triggers enhanced $Ca_V\beta_{2a}$-paGFP clustering and potentially increases $Ca_V1.2$ channel abundance at the sarcolemma.

ISO increases sarcolemmal expression of the pore-forming α_{1c} subunit in heart lysates

Biochemical techniques were employed to more directly test the postulate that ISO increases sarcolemmal $Ca_V1.2$ channel expression. Using differential centrifugation, we isolated plasma membrane and internal membrane fractions from whole heart lysates extracted from mice killed 20 min post-I.P. injection of saline (control) or 10 mg kg^{-1} ISO. Detection of insulin receptor β was used to confirm the identity of the plasma membrane fraction, and the presence of endosomal membranes in the internal membrane fraction was corroborated by detection of Rab4A. Consistent with the hypothesis that a PKA-dependent, readily-insertable pool of $Ca_V1.2$ channels forms sarcolemmal super-clusters, western blots revealed that ISO induced a 28.1 ± 0.1% increase in $Ca_V1.2$ channel expression in the plasma membrane (control: $N = 6$, ISO: $N = 7$, $P = 0.03$) (Fig. 4*G*) and an almost equivalent, reciprocal ~21% decrease in the amount of $Ca_V1.2$ in the internal membrane fraction (control: $N = 7$, ISO: $N = 6$, $P = 0.12$) (Fig. 4*H*). Collectively, these western blots results, along with our super-resolution and dynamic imaging experiments, confirm that $Ca_V1.2$ channel expression in the sarcolemma is augmented in response to βAR stimulation with ISO.

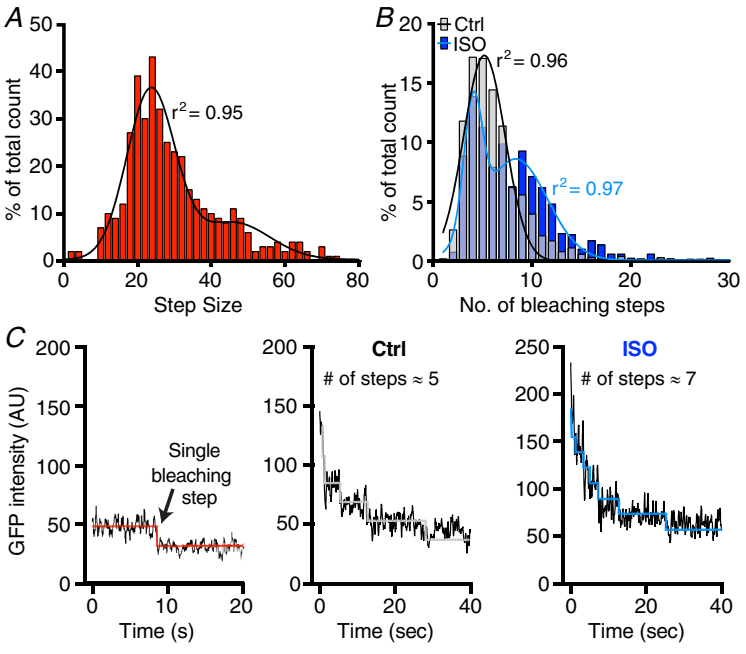

Figure 5. ISO treatment increases stepwise photobleaching assessed $Ca_V1.2$ channel cluster size
A, frequency distribution of photobleaching step sizes measured experiments performed on $Ca_V\beta_{2a}$-paGFP transduced myocytes. The data were well-fit (r^2 value shown) by a two-component Gaussian function with peaks at ~23 and 46 representing the fluorescence intensity change attributable to one and two-GFPs bleaching, respectively. *B*, frequency distribution of bleaching steps obtained from histogram $Ca_V\beta_{2a}$-paGFP transduced myocytes under control unstimulated conditions (grey; fit with a single Gaussian) or after application of 100 nM ISO (blue; fit with a two-component Gaussian). *C*, examples of bleaching steps for $Ca_V\beta_{2a}$-paGFP associated with $Ca_V1.2$ channels.

ISO induced super-clustering of $Ca_V1.2$ promotes enhanced co-operativity and amplifies Ca^{2+} influx in tsA-201 cells

We next aimed to determine whether the ISO-stimulated nanostructural rearrangement of $Ca_V1.2$ channels has any appreciable consequences for channel function. We predicted that the increased proximity of channels within larger super-clusters could favour co-operative interactions of the channels. We tested this prediction initially in transiently transfected tsA-201 cells by examining the single $Ca_V1.2$ channel activity using electrophysiological (cell-attached patch clamp) approaches (Fig. 6). The utility of heterologous expressions systems in the study of βAR of $Ca_V1.2$ channels is debatable. Several studies have noted that current augmentation in response to β-agonists is unreliable and less vigorous in these models than in cardiomyocytes (Perez-Reyes *et al.*, 1994; Charnet *et al.*, 1995; Zong *et al.*, 1995; Gao *et al.*, 1997; Weiss *et al.*, 2013). Indeed, we also had variable success in reproducing βAR regulation of $Ca_V1.2$ in tsA-201 cells, although we were able to do so in three separate cells where we observed augmented calcium currents and the characteristic leftward shift in current–voltage relationship (Fig. 7*A*–*C*). However, many tens of cells failed to show the response. In the cells that did respond, the fold-increase in peak current for each individual cell was 1.65, 1.49 and 1.42. These values are similar to the 1.6- to 2.8-fold increase in activity observed routinely in cardiomyocytes in the present study (1.63 ± 0.10-fold increase, $N = 3$, $n = 8$) (Fig. 8*A*–*C*) and in previous studies (Muth *et al.*, 1999; Lemke *et al.*, 2008; Nichols *et al.*, 2010; Brandmayr *et al.*, 2012) and suggest that a reasonable, albeit unreliable, βAR-mediated augmentation of current is achievable in these cells. Intriguingly, in the cell-attached patch configuration, we noted that augmentations in channel activity occurred much more reliably such that 55.6% of sampled patches displayed increased activity in response to ISO. Therefore, to be included in our analysis regimes, we set the criteria that, cells would have to display an increase in NP_o in response to ISO and exhibit multichannel

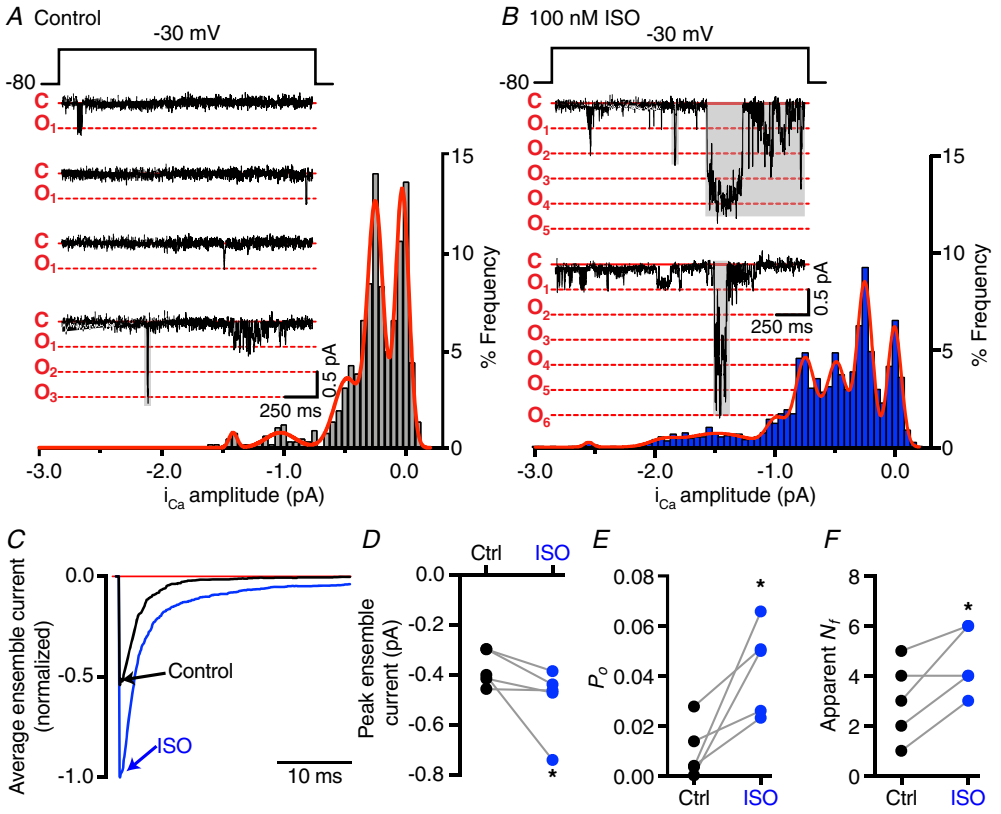

Figure 6. Co-operative gating behaviour of heterologously expressed $Ca_V1.2$ channels is promoted by ISO
A and *B*, representative i_{Ca} traces and accompanying amplitude histograms from tsA-201 cells expressing $Ca_V1.2$ during depolarization steps from –80 mV to –30 mV before (*A*) and during the application of 100 nM ISO (*B*). Note that traces in (*B*) are from the same cell as those in (*A*). Grey boxes highlight overt co-operative gating episodes. Amplitude histograms for control and ISO were fit with multicomponent Gaussian functions (red lines). *C*, current averaged over multiple sweeps performed on the cell shown in (*A*) and (*B*). *D*–*F*, paired symbol and line plots showing the peak ensemble current (*D*), P_o (*E*) and apparent N_f (*F*) for five cells before and during ISO application.

openings. Accordingly, using Ca^{2+} as the charge carrier, voltage steps from –80 mV to –30 mV were used to elicit $Ca_V1.2$ channel openings with a unitary amplitude of -0.47 ± 0.03 pA (Fig. 6*A*). Application of 100 nM ISO resulted in increased activity of the channels in the patch (Fig. 6*B*) but did not alter the unitary amplitude of the single channel current, which remained at 0.51 ± 0.02 pA ($P = 0.27$). Ensemble currents constructed by averaging single channel events before or in the presence of ISO, had activation and inactivation time courses commensurate with macroscopic currents (Fig. 6*C*). On average, a 1.34-fold increase in the ensemble current amplitude was observed after ISO ($n = 5$, $P = 0.03$) (Fig. 6*D*).

Macroscopic current (I_{Ca}) is the product of unitary current amplitude (i_{Ca}), open probability (P_o) and the number of functional channels (N_f). Because i_{Ca} did not change, we examined the other two variables. Application of ISO produced a 4-fold increase in P_o (0.01 ± 0.005 to 0.04 ± 0.008; $n = 5$, $P = 0.01$) (Fig. 6*E*) and a 1.5-fold increase in N_f (3 ± 1 to 5 ± 1, $n = 5$, $P = 0.03$) (Fig. 6*F*). Intriguingly, in many instances, we noted that depolarization in the presence of ISO revealed the concerted opening and closing of multiple channels (Fig. 6*B*, grey boxes). It is highly improbable that such temporally correlated multichannel openings could occur if these channels were only capable of acting as single, independently gating units. Instead, this behaviour suggests communication between the channels in the patch such that the opening of one channel can influence and co-ordinate the gating behaviour of its neighbors, leading to co-operative channel interactions.

The increase in N_f was further investigated by examining gating currents in $Ca_V1.2$-expressing tsA-201 cells before and after 100 nM ISO (Fig. 7*D–F*). Because ionic current was not blocked, we recorded gating currents at the reversal potential where ion flux is nil. Depolarizing pulses to E_{rev} should move the maximal gating charge, which is proportional to the total number of $Ca_V1.2$ channels expressed in the membrane of the cell according to the relationship $Q_{ON} = N \times q$ (where Q_{ON} is the time integral of the 'ON'gating charge and N is the number of channels in the membrane). A 16.7% increase in the number of channels in the membrane was found to occur upon application of ISO ($n = 5$) (Fig. 7*F*). These data are consistent with our live cell imaging observations

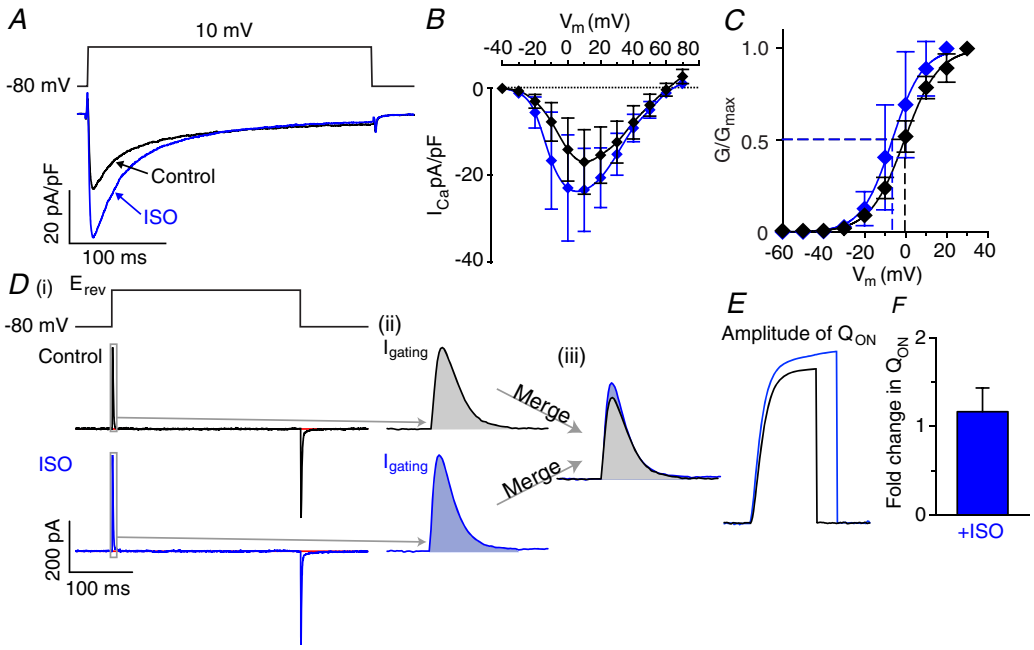

Figure 7. β-AR stimulation increases the number of functional channels in tsA-201 cell membranes
A, representative whole cell currents elicited from a $Ca_V1.2$-expressing tsA-201 cell during a 300 ms depolarization step from –80 mV to +10 mV before (control: black) and during application of 100 nM ISO (blue). *B*, I–V plot summarizing the results from $n = 3$ cells that displayed an ISO-stimulated increase in I_{Ca} with voltage steps from a holding potential of –80 mV to test potentials ranging from –40 mV to +70 mV. Currents were normalized to the cell capacitance to generate the current density. *C*, voltage-dependence of the normalized conductance (G/G_{max}) before and during ISO application, fit with Boltzmann functions. *D*, gating currents (I_{gating}) recorded from a $Ca_V1.2$-expressing tsA-201 cell during a 300 ms depolarizing step from -80 mV to the reversal potential (E_{rev}), before (black) and during application of 100 nM ISO (blue). Grey boxes in (i) indicate the ON I_{gating}, magnified in (ii) and merged for comparison in (iii). Shading beneath the ON I_{gating} indicates the area that was integrated to obtain the ON gating charge (Q_{ON}) shown in (*E*). *F*, fold-change in Qon during ISO application in $n = 5$ cells.

and suggest that activation of βARs is associated with an increase in the number of $Ca_V1.2$ channels in the plasma membrane.

Next, we recorded Ca^{2+} sparklets from transiently transfected tsA-201 cells. Using this optical approach, we can visualize channel openings over the entire TIRF-footprint of the cell (Navedo *et al.*, 2005; Nystoriak *et al.*, 2013). This presents a broader view of the single channel activity in the cell than the limited one we obtain within the confines of cell-attached patches. As shown in Supporting information (Movie S2), the utility of this approach is validated because many sites can identified throughout the cell footprint where there are no apparent functional channels, whereas other sites are quiescent under control conditions but become active after application of ISO. Consistent with our electrophysiology data, application of ISO increased $Ca_V1.2$ channel activity (nP_s) 3-fold (from 0.10 ± 0.03 to 0.30 ± 0.32, $n = 6$ and 4, respectively) (Fig. 9*A*–*C*). We observed an increase in activity in all patches exposed to ISO. The number of active sparklet sites per μm^2 (i.e. sparklet density) increased 2.5-fold with ISO, from 0.02 ± 0.005 to 0.05 ± 0.01 sites μm^{-2} ($P = 0.009$) (Fig. 9*D*). We analysed these sparklet traces using a coupled Markov chain model to obtain a measure of the co-operativity of the channel gating (e.g. coupling coefficient, κ) underlying these discrete calcium influx events. κ values lie within a 0–1 range, where a 0 value indicates channels that always gate independently and 1 indicates channels that always gate together in multichannel groups (Navedo *et al.*, 2010). Thus, any $\kappa > 0$ indicates some degree of co-operativity. The mean κ value of sparklet events was significantly higher after the application of ISO suggesting increased levels of co-operative gating behaviour ($P = 0.03$). This conclusion is also supported by the overtly co-operative behaviour, with several channels opening and/or closing in unison as seen in the representative traces in Fig. 9*B*. Collectively, these data suggest that application of ISO promotes increased activity and co-operativity between groups of $Ca_V1.2$ channels in tsA-201 cells. This creates localized regions of very high activity channels, which permits the influx of relatively large amounts of Ca^{2+} compared to that seen at the same site in the unstimulated cell.

ISO promotes co-operative gating behaviour and amplified Ca^{2+} influx in ventricular myocytes

Although we were able to occasionally observe reconstituted PKA modulation of recombinant $Ca_V1.2$ channels in tsA-201 cells, the lack of robust and reproducible increase in I_{Ca} upon application of ISO (except for the three cells mentioned above) is in agreement with the results of previous studies (Perez-Reyes *et al.*, 1994; Zong *et al.*, 1995; Gao *et al.*, 1997; Weiss *et al.*, 2013) and invites the criticism that any mechanistic insight gleaned from experiments in heterologous expression systems may not necessarily align with the mechanism at play in ventricular myocytes. We therefore turned our attention to freshly isolated adult mouse ventricular myocytes. If these same phenomena were to occur in ventricular myocytes during fight-or-flight, this could provide a means to tune Ca^{2+} influx to meet increased haemodynamic and metabolic demands. Therefore, we next measured elementary $Ca_V1.2$ channel currents from ventricular myocytes, before and after application of 100 nM ISO during a step depolarization to –30 mV (Fig. 10*A* and *B*). Unitary current amplitude was –0.44 ± 0.10 pA under control conditions and remained at a similar level (–0.49 ± 0.01 pA) after application of ISO ($P = 0.4376$, $n = 6$, $N = 5$) (Fig. 10*A* and *B*). As in tsA-201 cells, application of ISO augmented channel activity, as reflected by a 2-fold increase in the peak amplitude of the average ensemble current from –0.42 ± 0.09 pA in control to –0.82 ± 0.08 pA in ISO ($P = 0.0076$) (Fig. 10*C* and *D*). Channel P_o increased from 0.01 ± 0.008 in control

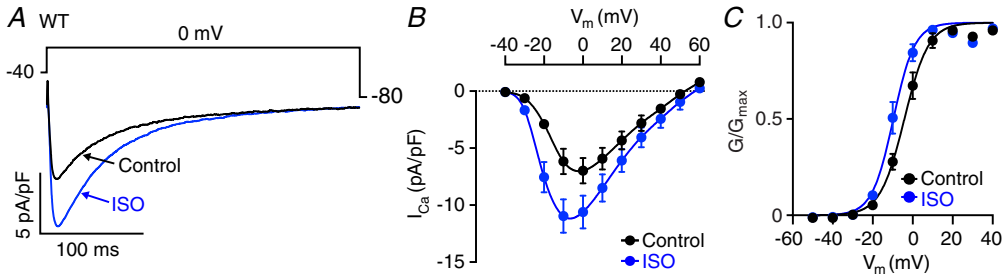

Figure 8. I_{Ca} are increased in isolated ventricular myocytes during β-AR stimulation
A, representative whole cell currents elicited from an adult ventricular myocyte during a 300 ms depolarization step from –40 mV to 0 mV before (control: black) and during application of 100 nM ISO (blue). *B*, *I–V* plot summarizing the results from $n = 8$ cells (from $N = 3$ animals) subjected to test potentials ranging from –40 mV to +60 mV. Currents were normalized to the cell capacitance to generate the current density. *C*, voltage-dependence of the normalized conductance (G/G_{max}) before and during ISO application, fit with Boltzmann functions.

to 0.11 ± 0.043 in ISO ($P = 0.016$) (Fig. 10*E*). We also found an ~2.5 fold increase in N_f from an average of 3 ± 1 channels in control to 8 ± 2 channels in ISO ($P = 0.02$) (Fig. 10*F*). We observed two distinct responses to ISO, with the majority of cells responding to ISO in a fashion similar to that displayed in Fig. 10*B* with large, simultaneous multichannel co-operative openings/closings occurring after ISO but with no obvious propensity towards a particular oligomeric state. One cell, however, displayed a strong preference for doublet channel openings after application of ISO (Fig. 10*G* and *H*), suggestive of a co-operative dimer of $Ca_V1.2$ channels, reminiscent of the recently reported dimeric preference of co-operatively gating $Na_V1.5$ channels (Clatot *et al.*, 2017). These data strongly support the hypothesis that ISO promotes co-operative interactions between $Ca_V1.2$ channels in ventricular myocytes.

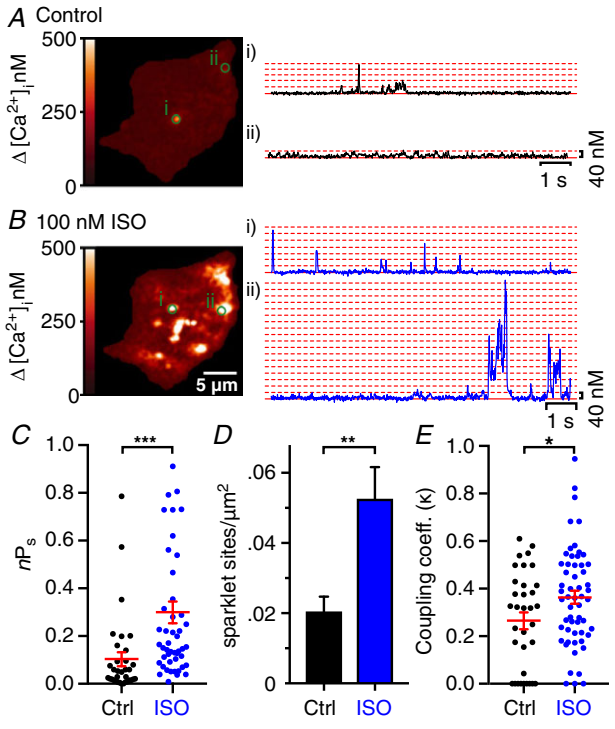

Figure 9. Optical recordings of ISO-induced augmentation in $Ca_V1.2$ channel co-operativity
A and *B*, calibrated TIRF images showing $Ca_V1.2$ channel-expressing, tsA-201 cell footprints, in a cell loaded with Rhod-2 Ca^{2+} indicator dye via the patch pipette. Images shown are maximum z-projections of image stacks recorded before (*A*) and during application of 100 nM ISO-stimulated (*B*). The time course of changes in $[Ca^{2+}]$ is shown on the right for two sparklet sites (denoted by green circles i and ii), before (black) and during ISO (blue). *C*–*E*, scatter and bar plots summarizing *nP*s (*C*), sparklet site density (*D*) and coupling coefficient (κ) (*E*) results obtained from $n = 6$ cells under control conditions and $n = 4$ cells in 100 nM ISO.

Discussion

Our data add a new level of understanding of βAR-mediated regulation of $Ca_V1.2$ channels and provide three novel insights into this phenomenon. We find that acute stimulation of βARs with ISO promotes: (i) enhanced physical, allosteric interactions between $Ca_V1.2$ channel C-terminal tails; (ii) a PKA-dependent, dynamic nanoscale redistribution of $Ca_V1.2$ channels, manifesting in super-clustering of the channels on the plasma membrane of cardiomyocytes and transfected tsA-201 cells; and (iii) an enhanced proximity between channels that facilitates co-operative interactions, leading to amplification of Ca^{2+} influx during fight-or-flight. We propose that this dynamic clustering and co-operativity response to ISO represents a newly appreciated means to tune EC-coupling in ventricular myocytes to meet acute increases in haemodynamic and metabolic demands during the fight-or-flight response.

A subsarcolemmal, presynthesized pool of channels to tune excitability?

In dynamic imaging experiments, we report that the response to ISO (increased $Ca_V\beta_{2a}$-paGFP F/F_0) could be detected immediately as the drug washed into the bath at room temperature (Fig. 4*C*), ruling out *de novo* protein synthesis and transport through the secretory pathway which takes more on the order of several minutes to hours (Lippincott-Schwartz *et al.*, 2000) and, instead, favouring a model in which a nearby sub-sarcolemmal pool of presynthesized $Ca_V1.2$ channels exists in cardiomyocytes. Dynamic insertion of β-subunit-associated channels into the sarcolemma at defined hubs could explain the super-clustering response to ISO seen in Fig. 2. An additional implication is that βAR activation triggers enhanced trafficking not only of the α_{1c}-pore forming subunit to the membrane, but also a possible co-transport of $Ca_V\beta_{2a}$-auxillary subunits. We cannot rule out the possibility that ISO increases the rate of dynamic association and dissociation of $Ca_V\beta_{2a}$ with the pore-forming α_{1c}. However, western blots showing enhanced α_{1c} expression at the sarcolemma post-ISO and super-resolution imaging data showing super-clustered α_{1c} post-ISO suggest that it is not only β-subunit mobilization that is altered in response to ISO.

β-subunits can themselves enhance $Ca_V1.2$ channel P_o via the formation of a rigid helix between the alpha interaction domain (AID) on the I–II loop of the α_{1c} and domain IS6 (Kanevsky & Dascal, 2006; Vitko *et al.*, 2008; Findeisen & Minor, 2009). In addition, β-subunits are known to influence $Ca_V1.2$ channel expression. How β-subunits exert this effect has been studied extensively. Initially, binding of β-subunits to the I–II loop of $Ca_V2.1$ was proposed to shield an endoplasmic reticulum

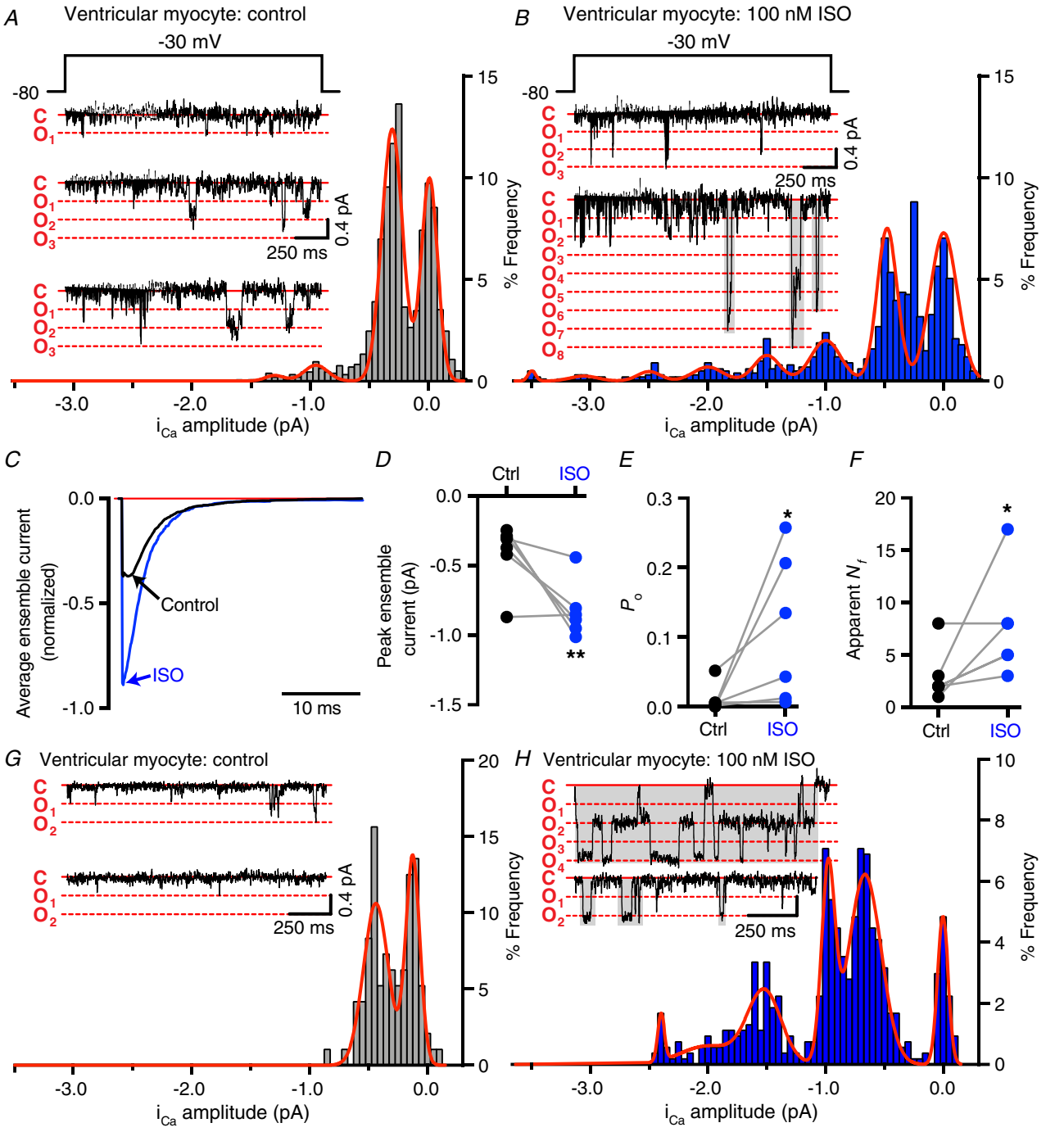

Figure 10. Elementary $Ca_V1.2$ channel currents are increased by ISO in adult ventricular myocytes
A and *B*, representative i_{Ca} traces elicited by a step depolarization from –80 mV to –30 mV before (control) (*A*) and during application of 100 nM ISO (*B*) each with amplitude histograms were fit with multicomponent Gaussian functions (red lines). *C*, average ensemble currents from the same cell before (black) and during ISO application (blue). *D–F*, paired symbol and line plots of the peak ensemble current (*D*), P_o (*E*) and apparent N_f (*F*) in $n = 6$, $N = 5$. *G* and *H*, i_{Ca} traces and accompanying amplitude histograms from a cell that displayed a preference for dimeric channel openings in the presence of ISO.

retention signal on the channel, thus promoting enhanced expression (Bichet *et al.*, 2000). However, the lack of an obvious endoplasmic reticulum retention motif on the I–II loop and data from subsequent studies led to the rejection of this idea and, instead, favoured the postulate that β-subunits protect $Ca_V1.2$ channels against proteasomal degradation and thus promote enhanced total channel protein and surface expression (Altier *et al.*, 2011; Waithe *et al.*, 2011). When the current manuscript was under consideration, an interesting study was published reporting that AID mutant $Ca_V1.2$ channels, unable to bind $Ca_V\beta$ subunits, are insensitive to βAR stimulation with ISO or the adenylyl cyclase activator forskolin. (Yang *et al.*, 2019). The results of the present study showing dynamic augmentation of $Ca_V1.2$ and $Ca_V\beta_{2a}$ sarcolemmal expression upon stimulation with ISO (Figs 2 and 4) have relevance to this work, and shed more light on the importance of the $Ca_V\beta$ subunit in adrenergic regulation of $Ca_V1.2$. Although the exact element in the pathway that responds to PKA phosphorylation to initiate this response remains unclear, it would be interesting to investigate whether phosphorylation of intracellular α_{1C} and/or $Ca_V\beta$, promotes an enhanced association between the two subunits, protecting α_{1C} from degradation, sustaining the sub-sarcolemmal pool, and promoting forward trafficking to the sarcolemma. If so, then this could be another previously unappreciated facet of βAR-mediated regulation of $Ca_V1.2$ channels.

In our model, channels within the readily insertable pool can be dispatched to the membrane in times of increased metabolic or haemodynamic demand. The volume of the pool therefore has direct implications for the magnitude of functional reserve that can be called upon to increase channel activity and inotropy in response to PKA-mediated channel phosphorylation. Additional questions that have not been explored in this initial study include: (i)) can the size of this pre-synthesized pool be increased by exercise training regimens to contribute to the larger βAR stimulated inotropic response seen in athletes and (ii) does the pool become depleted during chronic βAR stimulation that is known to occur in heart failure and/or myocardial ageing?

There is precedent for such a readily insertable pool of ion channels. In cardiomyocytes, an intracellular compartment of KCNQ1 channels is assumed to lie close to the Z-lines and can be mobilized to the sarcolemmal crest in response to elevations in $[Ca^{2+}]_i$ or stress, where they co-assemble with KCNE1 and form functional I_{Ks} channels, providing a repolarization reserve (Wang *et al.*, 2013; Jiang *et al.*, 2017). Additionally, in neurons, $[Ca^{2+}]_i$ and more specifically, influx of Ca^{2+} through $Ca_V1.2$ channels, is considered to regulate $Ca_V1.2$ channel trafficking and endocytosis to tune excitability there (Green *et al.*, 2007; Hall *et al.*, 2013). Furthermore, phosphorylation of the AMPAR subunit GluA1 at Ser^{845} by PKA and/or calcium/calmodulin-dependent protein kinase II, or PKC at Ser^{831}, promotes plasma membrane insertion of the receptors, facilitating long-term potentiation by increasing channel P_o and homeostatic scaling up (Makino *et al.*, 2011; Diering *et al.*, 2016; Olivito *et al.*, 2016). Conversely, dephosphorylation by calcineurin leads to receptor internalization, long-term depression and homeostatic scaling down (Lee *et al.*, 1998). A pool of intracellular GluA1-containing AMPARs is assumed to transition to a readily insertable state upon phosphorylation (Makino *et al.*, 2011). In a striking parallel, we find that PKA-mediated phosphorylation of $Ca_V1.2$ channels, downstream of βAR activation, leads to increased insertion of these channels into the cardiomyocyte sarcolemma. In the presence of PKA inhibitors (H-89 or PKI), the significant super-clustering response to ISO was abolished, implying that PKA activity is needed for this dynamic augmentation of $Ca_V1.2$ cluster size. Although PKA appears to be necessary and sufficient for the initiation of the super-clustering response to ISO, it remains to be determined whether other kinases, such as calmodulin-dependent protein kinase II or PKC, can generate a similar nanoscale redistribution of channels and super-clustering response.

Size of the functional reserve pool of channels

In many of our datasets, we observed a 'reserve' of ~17–45% of channels that could be mobilized to the membrane in response to ISO: (i) in super-resolution experiments, a 17% increase in mean $Ca_V1.2$ cluster area was observed in ISO-treated cardiomyocytes; (ii) in dynamic imaging experiments, ISO increased $Ca_V\beta_{2a}$-paGFP intensity in the sarcolemma by ~45%; (iii) in western experiments, ISO produced a 28% increase in the expression of $Ca_V1.2$ in the plasma membrane; and (iv) in stepwise photobleaching experiments, ISO increased the mean number of $Ca_V\beta_{2a}$-paGFP per cluster by 32%. Could this be the size of the functional reserve? The size of this putative channel reserve pool is not directly proportional to the 1.6- to 2.8-fold βAR-mediated increase in $Ca_V1.2$ macroscopic current routinely observed in ventricular myocytes (Muth *et al.*, 1999; Lemke *et al.*, 2008; Nichols *et al.*, 2010; Brandmayr *et al.*, 2012). However, as noted earlier, a small number of high P_o phosphorylated channels may have a disproportionately large effect on I_{Ca} if they interact with other non-phosphorylated channels in channel clusters (Dixon *et al.*, 2012). In an interesting parallel, a previous study performed on cortical neurons reported that 76% of $Ca_V1.2$ channels are on the cell surface (Green *et al.*, 2007), whereas the remaining 24% occupied intracellular locations. Do neurons then have a similarly sized functional reserve? Phosphorylation

of neuronal $Ca_V1.2$ channels is considered to play a role in $Ca_V1.2$ trafficking and stabilization at the membrane (Folci *et al.*, 2018), although, to our knowledge, the effect on channel cluster size remains to be clarified.

$Ca_V1.2$ channel trafficking: single channels or groups?

In support of our model, we recently reported that FP-tagged $Ca_V1.2$ channels are trafficked in vesicles within tsA-201 cells where they exhibit robust intracellular and submembrane movement (Ghosh *et al.*, 2018). In that study, we found that the diverse trafficking patterns of $Ca_V1.2$ required both microtubules (MTs) and an intact actin cytoskeleton. In cardiomyocytes, both of these scaffolding and transport elements have been postulated to play a role in $Ca_V1.2$ trafficking. There, a 'targeted delivery' model has been proposed for two channels: connexin 43 and $Ca_V1.2$ (Shaw *et al.*, 2007; Hong *et al.*, 2010; Chkourko *et al.*, 2012; Hong *et al.*, 2012; Xiao & Shaw, 2015). In this model, vesicular channel cargo enters the negative-end of the MT at the Golgi and is transported to defined delivery hubs at the plasma membrane where the MT plus-end binds to an anchor complex (Xiao & Shaw, 2015). In the case of $Ca_V1.2$ channels, BIN1 is the anchor/hub which docks the MT plus-end, targeting the channels to the t-tubule membrane (Hong *et al.*, 2010; Hong *et al.*, 2012). BIN1 interacts with non-sarcomeric actin (F-actin) to bind to α-actinin at the Z-lines, forming the anchor complex (Hong *et al.*, 2014). α-actinin itself is known to play a role in promoting $Ca_V1.2$ channel expression and function at the membrane (Hall *et al.*, 2013; Tseng *et al.*, 2017). Although, in the present study, our methodology did not permit imaging of the pore-forming subunit of the channels directly in cardiomyocytes, we did observe dynamic insertion of FP-tagged $Ca_V\beta_{2a}$ into the membrane in response to ISO (Fig. 4; see also the Supporting information, Movie S1). Notably, we observe that these insertions are not limited to single channels but frequently involve larger clusters of multiple channels. An interesting finding in the present study that lends credence to this idea arises when we consider the apparently counterintuitive kinetics of the BiFC experiments (Fig. 1). It might be predicted that, because ISO increases the likelihood of channel interactions, it should then increase the kinetics of venus reconstitution in the BiFC assayed response. However, we saw quite the opposite. ISO-sensitive $Ca_V1.2$–$Ca_V1.2$ channel interactions, although larger in magnitude, occurred on a notably slower time scale ($\tau = 35.76$ min) than those occurring spontaneously in unstimulated cells ($\tau = 18.57$ min). One possible explanation for this slower rate is that the more complex signalling pathway required to stimulate the ISO-sensitive interactions simply requires more time (i.e. the τ reflects the time taken for β_2-AR activation, signalling, channel phosphorylation, subsequent physical interactions and maturation of the newly constituted venus fluorescence). Because we performed these experiments in TIRF mode, any readout is probably in or very close to the plasma membrane of the cells. Thus, an alternative explanation is that the longer timescale for the ISO-sensitive interactions reflects the time taken for $Ca_V1.2$ channels, interacting with one another in intracellular vesicles, to be trafficked to the surface where they would then be evident in our TIRF footprint. This second explanation is supported by dynamic imaging results where we captured 'new' clusters of $Ca_V\beta_{2a}$ appearing in myocyte TIRF footprints in response to ISO. Our biochemical expression studies lend further credence to this model, revealing an ISO-stimulated augmentation of a plasma membrane pool of cardiac $Ca_V1.2$ channels with a coincident, and almost equal magnitude depletion of an intracellular membrane pool. At least two open questions remain; first does PKA phosphorylate sarcolemmal and/or vesicular $Ca_V1.2$? Our model supports phosphorylation of an internal pool of channels which results in enhanced targeting and insertion of those channels to the sarcolemma. The second question considers the internalized pool of functionally viable β_1 and β_2-ARs that has been reported in recent years (Irannejad *et al.*, 2013; Irannejad *et al.*, 2017). Can these internalized βARs signal to phosphorylate intracellular $Ca_V1.2$, promoting their membrane targeting? Future studies should pursue answers to these questions.

Impact of super-clustering on EC-coupling

Although we do not explicitly investigate the effect of super-clustering on EC-coupling in the present study, considering the indispensable role played by $Ca_V1.2$ channels in this vital process, it merits some discussion. In a previous study, we utilized a light activated dimerization strategy to force channels to physically interact, and found that $Ca_V1.2$–$Ca_V1.2$ contact resulted in increased co-operative gating and amplification of whole-cell I_{Ca}, resulting in larger $[Ca^{2+}]_i$ transients in adult rat ventricular myocytes (Dixon *et al.*, 2012). We have also confirmed and recapitulated these effects of channel co-operativity in a recent *in silico* study (Sato *et al.*, 2018). Thus, $Ca_V1.2$ clustering and co-operative gating can increase Ca^{2+} influx to the point where it has a tangible effect on excitability. One would predict that the most impactful effect on EC-coupling and inotropy would be produced by preferentially localizing $Ca_V1.2$ channel super-clusters at positions opposite type 2 ryanodine receptor clusters on the junctional sarcoplasmic reticulum. Phosphorylated type 2 ryanodine receptors have been reported by others to display enhanced dyad-localized clustering in response to ISO (Fu *et al.*, 2016). Future studies should investigate the juxta-positioning of these

two augmented cluster populations and the effect on EC-coupling.

In conclusion, the present study reveals a newly appreciated facet of the mechanism underlying βAR mediated regulation of $Ca_V1.2$ channels. We present a revised model in which βAR activation initiates a PKA-dependent dynamic augmentation of $Ca_V1.2$ channel expression on the sarcolemma of ventricular myocytes, facilitating their co-operative interactions, and amplifying Ca^{2+} influx. This adds a new layer of complexity to our understanding of adrenergic regulation of these channels, and could provide a means to fine tune EC-coupling to meet acutely increased haemodynamic and metabolic demands during fight-or-flight.

References

Altier C, Garcia-Caballero A, Simms B, You H, Chen L, Walcher J, Tedford HW, Hermosilla T & Zamponi GW (2011). The $Ca_V\beta$ subunit prevents RFP2-mediated ubiquitination and proteasomal degradation of L-type channels. *Nat Neurosci* **14**, 173–180.

Atwood BK, Lopez J, Wager-Miller J, Mackie K & Straiker A (2011). Expression of G protein-coupled receptors and related proteins in HEK293, AtT20, BV2, and N18 cell lines as revealed by microarray analysis. *BMC Genomics* **12**, 14.

Bean BP, Nowycky MC & Tsien RW (1984). Beta-adrenergic modulation of calcium channels in frog ventricular heart cells. *Nature* **307**, 371–375.

Bhargava A, Lin X, Novak P, Mehta K, Korchev Y, Delmar M & Gorelik J (2013). Super-resolution scanning patch clamp reveals clustering of functional ion channels in adult ventricular myocyte. *Circ Res* **112**, 1112–1120.

Bichet D, Cornet V, Geib S, Carlier E, Volsen S, Hoshi T, Mori Y & De Waard M (2000). The I-II loop of the Ca^{2+} channel α_1 subunit contains an endoplasmic reticulum retention signal antagonized by the beta subunit. *Neuron* **25**, 177–190.

Brandmayr J, Poomvanicha M, Domes K, Ding J, Blaich A, Wegener JW, Moosmang S & Hofmann F (2012). Deletion of the C-terminal phosphorylation sites in the cardiac beta-subunit does not affect the basic beta-adrenergic response of the heart and the $Ca_V1.2$ channel. *J Biol Chem* **287**, 22584–22592.

Buonarati OR, Henderson PB, Murphy GG, Horne MC & Hell JW (2017). Proteolytic processing of the L-type Ca^{2+} channel $\alpha_1 1.2$ subunit in neurons. *F1000Res* **6**, 1166.

Charnet P, Lory P, Bourinet E, Collin T & Nargeot J (1995). cAMP-dependent phosphorylation of the cardiac L-type Ca channel: a missing link? *Biochimie* **77**, 957–962.

Chen-Izu Y (2010). Multiple levels of the single L-type Ca^{2+} channel conductance in adult mammalian ventricular myocytes. *Biochem Biophys Res Commun.* **391**, 604–608.

Cheng EP, Yuan C, Navedo MF, Dixon RE, Nieves-Cintron M, Scott JD & Santana LF (2011). Restoration of normal L-type Ca^{2+} channel function during Timothy syndrome by ablation of an anchoring protein. *Circ Res* **109**, 255–261.

Chkourko HS, Guerrero-Serna G, Lin X, Darwish N, Pohlmann JR, Cook KE, Martens JR, Rothenberg E, Musa H & Delmar M (2012). Remodeling of mechanical junctions and of microtubule-associated proteins accompany cardiac connexin43 lateralization. *Heart Rhythm* **9**, 1133–1140 e1136.

Clatot J, Hoshi M, Wan X, Liu H, Jain A, Shinlapawittayatorn K, Marionneau C, Ficker E, Ha T & Deschenes I (2017). Voltage-gated sodium channels assemble and gate as dimers. *Nat Commun* **8**, 2077.

Dalton S, Takahashi SX, Miriyala J & Colecraft HM (2005). A single $Ca_V\beta$ can reconstitute both trafficking and macroscopic conductance of voltage-dependent calcium channels. *J Physiol* **567**, 757–769.

Davare MA, Horne MC & Hell JW (2000). Protein phosphatase 2A is associated with class C L-type calcium channels ($Ca_V1.2$) and antagonizes channel phosphorylation by cAMP-dependent protein kinase. *J Biol Chem* **275**, 39710–39717.

Diering GH, Heo S, Hussain NK, Liu B & Huganir RL (2016). Extensive phosphorylation of AMPA receptors in neurons. *Proc Natl Acad Sci U S A* **113**, E4920–E4927.

Dixon RE, Moreno CM, Yuan C, Opitz-Araya X, Binder MD, Navedo MF & Santana LF (2015). Graded Ca^{2+}/calmodulin-dependent coupling of voltage-gated $Ca_V1.2$ channels. *Elife* **4**, e05608.

Dixon RE, Vivas O, Hannigan KI & Dickson EJ (2017). Ground state depletion super-resolution imaging in mammalian cells. *J Vis Exp* **129**, e56239.

Dixon RE, Yuan C, Cheng EP, Navedo MF & Santana LF (2012). Ca^{2+} signaling amplification by oligomerization of L-type $Ca_V1.2$ channels. *Proc Natl Acad Sci U S A* **109**, 1749–1754.

Drum BM, Dixon RE, Yuan C, Cheng EP & Santana LF (2013). Cellular mechanisms of ventricular arrhythmias in a mouse model of Timothy syndrome (long QT syndrome 8). *J Mol Cell Cardiol* **66C**, 63–71.

Drum BM, Yuan C, Li L, Liu Q, Wordeman L & Santana LF (2016). Oxidative stress decreases microtubule growth and stability in ventricular myocytes. *J Mol Cell Cardiol* **93**, 32–43.

Fang H, Lai NC, Gao MH, Miyanohara A, Roth DM, Tang T & Hammond HK (2012). Comparison of adeno-associated virus serotypes and delivery methods for cardiac gene transfer. *Hum Gene Ther Methods* **23**, 234–241.

Findeisen F & Minor DL, Jr (2009). Disruption of the IS6-AID linker affects voltage-gated calcium channel inactivation and facilitation. *J Gen Physiol* **133**, 327–343.

Folci A, Steinberger A, Lee B, Stanika R, Scheruebel S, Campiglio M, Ramprecht C, Pelzmann B, Hell JW, Obermair GJ, Heine M & Di Biase V (2018). Molecular mimicking of C-terminal phosphorylation tunes the surface dynamics of $Ca_V1.2$ calcium channels in hippocampal neurons. *J Biol Chem* **293**, 1040–1053.

Franzini-Armstrong C, Protasi F & Ramesh V (1998). Comparative ultrastructure of Ca^{2+} release units in skeletal and cardiac muscle. *Ann NY Acad Sci* **853**, 20–30.

Fu Y, Shaw SA, Naami R, Vuong CL, Basheer WA, Guo X & Hong T (2016). Isoproterenol promotes rapid ryanodine receptor movement to bridging integrator 1 (BIN1)-organized dyads. *Circulation* **133**, 388–397.

Gao T, Yatani A, Dell'Acqua ML, Sako H, Green SA, Dascal N, Scott JD & Hosey MM (1997). cAMP-dependent regulation of cardiac L-type Ca^{2+} channels requires membrane targeting of PKA and phosphorylation of channel subunits. *Neuron* **19**, 185–196.

Ghosh D, Nieves-Cintron M, Tajada S, Brust-Mascher I, Horne MC, Hell JW, Dixon RE, Santana LF & Navedo MF (2018). Dynamic L-type $Ca_V1.2$ channel trafficking facilitates $Ca_V1.2$ clustering and cooperative gating. *Biochim Biophys Acta* **1865**, 1341–1355.

Green EM, Barrett CF, Bultynck G, Shamah SM & Dolmetsch RE (2007). The tumor suppressor eIF3e mediates calcium-dependent internalization of the L-type calcium channel $Ca_V1.2$. *Neuron* **55**, 615–632.

Grundy D (2015). Principles and standards for reporting animal experiments in The Journal of Physiology and Experimental Physiology. *J Physiol* **593**, 2547–2549.

Gustafsson N, Culley S, Ashdown G, Owen DM, Pereira PM & Henriques R (2016). Fast live-cell conventional fluorophore nanoscopy with ImageJ through super-resolution radial fluctuations. *Nat Commun* **7**, 12471.

Hall DD, Dai S, Tseng PY, Malik Z, Nguyen M, Matt L, Schnizler K, Shephard A, Mohapatra DP, Tsuruta F, Dolmetsch RE, Christel CJ, Lee A, Burette A, Weinberg RJ & Hell JW (2013). Competition between α-actinin and Ca^{2+}-calmodulin controls surface retention of the L-type Ca^{2+} channel $Ca_V1.2$. *Neuron* **78**, 483–497.

Hartzell HC, Mery PF, Fischmeister R & Szabo G (1991). Sympathetic regulation of cardiac calcium current is due exclusively to cAMP-dependent phosphorylation. *Nature* **351**, 573–576.

Hidaka H & Kobayashi R (1992). Pharmacology of protein kinase inhibitors. *Annu Rev Pharmacol Toxicol* **32**, 377–397.

Hong T, Yang H, Zhang SS, Cho HC, Kalashnikova M, Sun B, Zhang H, Bhargava A, Grabe M, Olgin J, Gorelik J, Marban E, Jan LY & Shaw RM (2014). Cardiac BIN1 folds T-tubule membrane, controlling ion flux and limiting arrhythmia. *Nat Med* **20**, 624–632.

Hong TT, Smyth JW, Chu KY, Vogan JM, Fong TS, Jensen BC, Fang K, Halushka MK, Russell SD, Colecraft H, Hoopes CW, Ocorr K, Chi NC & Shaw RM (2012). BIN1 is reduced and $Ca_V1.2$ trafficking is impaired in human failing cardiomyocytes. *Heart Rhythm* **9**, 812–820.

Hong TT, Smyth JW, Gao D, Chu KY, Vogan JM, Fong TS, Jensen BC, Colecraft HM & Shaw RM (2010). BIN1 localizes the L-type calcium channel to cardiac T-tubules. *PLoS Biol* **8**, e1000312.

Irannejad R, Pessino V, Mika D, Huang B, Wedegaertner PB, Conti M & von Zastrow M (2017). Functional selectivity of GPCR-directed drug action through location bias. *Nat Chem Biol* **13**, 799–806.

Irannejad R, Tomshine JC, Tomshine JR, Chevalier M, Mahoney JP, Steyaert J, Rasmussen SG, Sunahara RK, El-Samad H, Huang B & von Zastrow M (2013). Conformational biosensors reveal GPCR signalling from endosomes. *Nature* **495**, 534–538.

Jiang M, Wang Y & Tseng GN (2017). Adult Ventricular myocytes segregate KCNQ1 and KCNE1 to keep the IK_s amplitude in check until when larger IK_s is needed. *Circ Arrhythm Electrophysiol* **10**, e005084.

Josephson IR, Guia A, Lakatta EG & Stern MD (2002). Modulation of the conductance of unitary cardiac L-type Ca^{2+} channels by conditioning voltage and divalent ions. *Biophys J* **83**, 2587–2594.

Kanevsky N & Dascal N (2006). Regulation of maximal open probability is a separable function of $Ca_V\beta$ subunit in L-type Ca^{2+} channel, dependent on NH_2 terminus of α_{1C} ($Ca_V1.2\alpha$). *J Gen Physiol* **128**, 15–36.

Kirkton RD & Bursac N (2011). Engineering biosynthetic excitable tissues from unexcitable cells for electrophysiological and cell therapy studies. *Nat Commun* **2**, 300.

Kodama Y & Hu CD (2010). An improved bimolecular fluorescence complementation assay with a high signal-to-noise ratio. *Biotechniques* **49**, 793–805.

Lee HK, Kameyama K, Huganir RL & Bear MF (1998). NMDA induces long-term synaptic depression and dephosphorylation of the GluR1 subunit of AMPA receptors in hippocampus. *Neuron* **21**, 1151–1162.

Lemke T, Welling A, Christel CJ, Blaich A, Bernhard D, Lenhardt P, Hofmann F & Moosmang S (2008). Unchanged beta-adrenergic stimulation of cardiac L-type calcium channels in $Ca_V1.2$ phosphorylation site S1928A mutant mice. *J Biol Chem* **283**, 34738–34744.

Lippincott-Schwartz J, Roberts TH & Hirschberg K (2000). Secretory protein trafficking and organelle dynamics in living cells. *Annu Rev Cell Dev Biol* **16**, 557–589.

Louch WE, Sheehan KA & Wolska BM (2011). Methods in cardiomyocyte isolation, culture, and gene transfer. *J Mol Cell Cardiol* **51**, 288–298.

Makino Y, Johnson RC, Yu Y, Takamiya K & Huganir RL (2011). Enhanced synaptic plasticity in mice with phosphomimetic mutation of the GluA1 AMPA receptor. *Proc Natl Acad Sci U S A* **108**, 8450–8455.

Maravall M, Mainen ZF, Sabatini BL & Svoboda K (2000). Estimating intracellular calcium concentrations and buffering without wavelength ratioing. *Biophys J* **78**, 2655–2667.

Moreno CM, Dixon RE, Tajada S, Yuan C, Opitz-Araya X, Binder MD & Santana LF (2016). Ca^{2+} entry into neurons is facilitated by cooperative gating of clustered $Ca_V1.3$ channels. *Elife* **5**, e15744.

Murray AJ (2008). Pharmacological PKA inhibition: all may not be what it seems. *Sci Signal* 3;**1**, re4.

Muth JN, Yamaguchi H, Mikala G, Grupp IL, Lewis W, Cheng H, Song LS, Lakatta EG, Varadi G & Schwartz A (1999). Cardiac-specific overexpression of the α_1 subunit of the L-type voltage-dependent Ca^{2+} channel in transgenic mice. Loss of isoproterenol-induced contraction. *J Biol Chem* **274**, 21503–21506.

Nagai T, Ibata K, Park ES, Kubota M, Mikoshiba K & Miyawaki A (2002). A variant of yellow fluorescent protein with fast and efficient maturation for cell-biological applications. *Nat Biotechnol* **20**, 87–90.

National Research Council (U.S.). Committee for the Update of the Guide for the Care and Use of Laboratory Animals., Institute for Laboratory Animal Research (U.S.) & National Academies Press (U.S.) (2011). *Guide for the Care and Use of Laboratory Animals*. National Academies Press, Washington, DC.

Navedo MF, Amberg GC, Votaw VS & Santana LF (2005). Constitutively active L-type Ca^{2+} channels. *Proc Natl Acad Sci U S A* **102**, 11112–11117.

Navedo MF, Cheng EP, Yuan C, Votaw S, Molkentin JD, Scott JD & Santana LF (2010). Increased coupled gating of L-type Ca^{2+} channels during hypertension and Timothy syndrome. *Circ Res* **106**, 748–756.

Nichols CB, Rossow CF, Navedo MF, Westenbroek RE, Catterall WA, Santana LF & McKnight GS (2010). Sympathetic stimulation of adult cardiomyocytes requires association of AKAP5 with a subpopulation of L-type calcium channels. *Circ Res* **107**, 747–756.

Nystoriak MA, Nieves-Cintron M & Navedo MF (2013). Capturing single L-type Ca^{2+} channel function with optics. *Biochim Biophys Acta* **1833**, 1657–1664.

Olivito L, Saccone P, Perri V, Bachman JL, Fragapane P, Mele A, Huganir RL & De Leonibus E (2016). Phosphorylation of the AMPA receptor GluA1 subunit regulates memory load capacity. *Brain Struct Funct* **221**, 591–603.

Osterrieder W, Brum G, Hescheler J, Trautwein W, Flockerzi V & Hofmann F (1982). Injection of subunits of cyclic AMP-dependent protein kinase into cardiac myocytes modulates Ca^{2+} current. *Nature* **298**, 576–578.

Perez-Reyes E, Yuan W, Wei X & Bers DM (1994). Regulation of the cloned L-type cardiac calcium channel by cyclic-AMP-dependent protein kinase. *FEBS Lett* **342**, 119–123.

Reuter H & Scholz H (1977). The regulation of the calcium conductance of cardiac muscle by adrenaline. *J Physiol* **264**, 49–62.

Robida AM & Kerppola TK (2009). Bimolecular fluorescence complementation analysis of inducible protein interactions: effects of factors affecting protein folding on fluorescent protein fragment association. *J Mol Biol* **394**, 391–409.

Rubart M, Patlak JB & Nelson MT (1996). Ca^{2+} currents in cerebral artery smooth muscle cells of rat at physiological Ca^{2+} concentrations. *J Gen Physiol* **107**, 459–472.

Sato D, Dixon RE, Santana LF & Navedo MF (2018). A model for cooperative gating of L-type Ca^{2+} channels and its effects on cardiac alternans dynamics. *PLoS Comput Biol* **14**, e1005906.

Shaw RM, Fay AJ, Puthenveedu MA, von Zastrow M, Jan YN & Jan LY (2007). Microtubule plus-end-tracking proteins target gap junctions directly from the cell interior to adherens junctions. *Cell* **128**, 547–560.

Sperelakis N & Schneider JA (1976). A metabolic control mechanism for calcium ion influx that may protect the ventricular myocardial cell. *Am J Cardiol* **37**, 1079–1085.

Tseng PY, Henderson PB, Hergarden AC, Patriarchi T, Coleman AM, Lillya MW, Montagut-Bordas C, Lee B, Hell JW & Horne MC (2017). α-Actinin promotes surface localization and current density of the Ca^{2+} channel $Ca_V1.2$ by binding to the IQ region of the α_1 subunit. *Biochemistry* **56**, 3669–3681.

Tsien RW, Giles W & Greengard P (1972). Cyclic AMP mediates the effects of adrenaline on cardiac purkinje fibres. *Nat New Biol* **240**, 181–183.

Ulbrich MH & Isacoff EY (2007). Subunit counting in membrane-bound proteins. *Nat Methods* **4**, 319–321.

Vinge LE, Raake PW & Koch WJ (2008). Gene therapy in heart failure. *Circ Res* **102**, 1458–1470.

Vitko I, Shcheglovitov A, Baumgart JP, Arias O, II, Murbartian J, Arias JM & Perez-Reyes E (2008). Orientation of the calcium channel beta relative to the $\alpha_1$2.2 subunit is critical for its regulation of channel activity. *PLoS ONE* **3**, e3560.

Waithe D, Ferron L, Page KM, Chaggar K & Dolphin AC (2011). Beta-subunits promote the expression of $Ca_V2.2$ channels by reducing their proteasomal degradation. *J Biol Chem* **286**, 9598–9611.

Wang Y, Zankov DP, Jiang M, Zhang M, Henderson SC & Tseng GN (2013). $[Ca^{2+}]_i$ elevation and oxidative stress induce KCNQ1 protein translocation from the cytosol to the cell surface and increase slow delayed rectifier (IK_s) in cardiac myocytes. *J Biol Chem* **288**, 35358–35371.

Weiss S, Oz S, Benmocha A & Dascal N (2013). Regulation of cardiac L-type Ca^{2+} channel $Ca_V1.2$ via the beta-adrenergic-cAMP-protein kinase A pathway: old dogmas, advances, and new uncertainties. *Circ Res* **113**, 617–631.

Xiao S & Shaw RM (2015). Cardiomyocyte protein trafficking: relevance to heart disease and opportunities for therapeutic intervention. *Trends Cardiovasc Med* **25**, 379–389.

Yang L, Katchman A, Kushner JS, Kushnir A, Zakharov SI, Chen BX, Shuja Z, Subramanyam P, Liu G, Papa A, Roybal DD, Pitt GS, Colecraft HM & Marx SO (2019). Cardiac $Ca_V1.2$ channels require beta subunits for beta-adrenergic-mediated modulation but not trafficking. *J Clin Invest* **129**, 647–658.

Yue DT, Herzig S & Marban E (1990). Beta-adrenergic stimulation of calcium channels occurs by potentiation of high-activity gating modes. *Proc Natl Acad Sci U S A* **87**, 753–757.

Zima AV, Picht E, Bers DM & Blatter LA (2008). Termination of cardiac Ca^{2+} sparks: role of intra-SR $[Ca^{2+}]$, release flux, and intra-SR Ca^{2+} diffusion. *Circ Res* **103**, e105-115.

Zong X, Schreieck J, Mehrke G, Welling A, Schuster A, Bosse E, Flockerzi V & Hofmann F (1995). On the regulation of the expressed L-type calcium channel by cAMP-dependent phosphorylation. *Pflugers Arch* **430**, 340–347.

Additional information

Competing interests

The authors declare that they have no competing interests.

Author contributions

RED conceived and designed the experiments. RED, DI, KIH, BX, DG and SGV executed the experiments. RED, DI, KIH BX and DG collected data. RED, DI, KIH and BX analysed the data. RED, YKX, EJD and MFN interpreted data. RED, DI, KIH and BX wrote the manuscript. RED, DI, KIH, BX, DG, SGV, YKX, EJD and MFN revised the manuscript. All authors approve the

final version of the manuscript for publication and agree to be accountable for all aspects of the work. All listed authors meet the requirements for authorship, and all those who qualify for authorship are listed.

Funding

This work was supported by AHA grants 15SDG25560035 (RED) and 18POST34060234 (DG); NIH NHLBI grants T32 HL086350 (DWI) and MFNs R01HL098200 and R01HL121059; and NIGMS grant R01GM127513 to EJD; and VA Merit grant 1I01BX002900 (YKX).

Acknowledgements

We wish to thank Dr Fernando Santana for the use of his GSD microscope, helpful discussions, and for providing insightful comments on our manuscript. We also thank Dr Johannes Hell for generously providing the anti-$Ca_V1.2$ FP1 antibody.

Supporting information

Additional supporting information may be found online in the Supporting Information section at the end of the article.

Movie S1. ISO stimulates dynamic augmentation of sarcolemmal $Ca_V\beta_{2a}$-paGFP expression in transduced ventricular myocytes

Movie S2. Ca^{2+} sparklet activity, site density and co-operativity are augmented by ISO